Contents lists available at ScienceDirect

Geomorphology

Lava deltas, a key landform in oceanic volcanic islands: El Hierro, Canary Islands

A. Rodriguez-Gonzalez [a], J.L. Fernandez-Turiel [b,*], M. Aulinas [c,d], M.C. Cabrera [a], C. Prieto-Torrell [c,d], G.A. Rodriguez [a], H. Guillou [e], F.J. Perez-Torrado [a]

[a] *Instituto de Estudios Ambientales y Recursos Naturales (iUNAT), Universidad de Las Palmas de Gran Canaria (ULPGC), Las Palmas de Gran Canaria, Spain*
[b] *Geosciences Barcelona, GEO3BCN, CSIC, Barcelona, Spain*
[c] *Departament de Mineralogia, Petrologia i Geologia Aplicada, Facultat de Ciències de la Terra, Universitat de Barcelona (UB), Spain*
[d] *Institut de Recerca Geomodels, Facultat de Ciències de la Terra, Universitat de Barcelona, Martí i Franquès s/n, Barcelona 08028, Spain*
[e] *Laboratoire des Sciences du Climat et de l'Environnement/IPSL, CEA-CNRS-UVSQ, Avenue de la Terrasse, 91198 Gif-sur-Yvette Cédex, France*

ARTICLE INFO

ABSTRACT

Marine and subaerial erosion of volcanic ocean islands form coastal cliffs and shore platforms, particularly during stable sea levels. Posterosional lava flows can spill over these coastal cliffs and fill the platforms, leading to the progradation of lava deltas. This work aims to analyze this volcanic rocky coast setting at the island scale and to assess the volcanic constructional and erosive degradational effects on the coast at the scale of one volcanic edifice. El Hierro Island, Canary Islands, exemplifies a rocky coast with an active sea-cliff profile, reflecting its early evolutionary stage as a young ocean volcanic island with no fringing reef. The occurrence of a contemporary insular shelf formed during the Holocene sea-level highstand (<7 ka) allows constraining the ages of those eruptions forming lava deltas affecting this geomorphological landform. A detailed bathymetry around the island allowed us to distinguish 17 eruptions fulfilling this criterion. The Montaña del Tesoro, which occurred about 1050 years BP, is one of these eruptions and was selected as a case study for morphometric modeling integrating subaerial and submarine data at the scale of a volcanic edifice. This eruption was a Strombolian basaltic volcanic event that produced a scoria cone, pyroclastic fall deposits, and lava flows that reached the ocean in the eastern rift zone of El Hierro island. We combine field-based observations with topographic and bathymetric data analysis to reconstruct the pre- and post-eruption Digital Elevation Models (DEMs) and, comparing with present-day DEM, to analyze morphometrically the influence of volcanism on the coastal landscape's development. The resulting landform complexity required the discretization of the lava field according to the coastline evolution and lava front sectors, and the subaerial or submarine lava placement. The pyroclastic materials' total erupted bulk volume (12,829,578 m^3) corresponds to a volcanic eruption index (VEI) of 3. This event was primarily effusive. From a dense rock equivalent (DRE) volume of 25,615,424 m^3, 87 % flowed as lava, 10 % formed the cinder cone, and 3 % the tephra fall deposits. We quantitatively demonstrate that dominant degradation occurs in the lava field, mainly disturbed by marine erosion. Marine erosion removed 9 % of the erupted volume of lava flows against 1 % by fluvial erosion. This work provides methods and results of great interest with different implications in oceanic volcanic islands, among which we can mention coastal planning (e.g., rock coast evolution) and volcanic risk assessment (e.g., the importance of Holocene sea-level rise on the development of shore platforms facilitating the progradation of lava deltas).

1. Introduction

Rocky coasts represent the majority of the world's shorelines (Stephenson et al., 2013; Woodroffe, 2014). Coastal cliffs likely exist on about 52 % of the global shoreline (Young and Carilli, 2019). Rocky shorelines are common on oceanic islands (Woodroffe, 2014), and on

---

* Corresponding author.
E-mail addresses: alejandro.rodriguezgonzalez@ulpgc.es (A. Rodriguez-Gonzalez), jlfernandez@geo3bcn.csic.es (J.L. Fernandez-Turiel), meritxellaulinas@ub.edu (M. Aulinas), mcarmen.cabrera@ulpgc.es (M.C. Cabrera), c.prieto-torrell@ub.edu (C. Prieto-Torrell), herve.guillou@lsce.ipsl.fr (H. Guillou), franciscojose.perez@ulpgc.es (F.J. Perez-Torrado).

those islands located on oceanic plates, volcanism is the most important geological process (Nunn, 1994).

Seawater penetrating lava flows are usual on ocean islands in hot spot archipelagos (Carracedo et al., 2001; Mattox and Mangan, 1997; Soule et al., 2021; Thouret, 1999). In this setting, the coastal landscape is the result of complex evolutions involving the interaction of aggradational (e.g., effusion, deposition) and degradational (e.g., terrestrial and marine erosion, deformation) processes, which therefore contribute effectively to the creation of the island's relief (Ramalho et al., 2013; Rodriguez-Gonzalez et al., 2011; Woodroffe, 2014).

During the emergent stage of volcanic ocean islands, volcanic constructional activity prevails, and coastal evolution is essentially driven by intermittent lateral growth through the formation of lava deltas (Ramalho et al., 2013; Soule et al., 2021). When the sea level is relatively stable, surface erosional processes form cliffs that, when retreat, leads to a rock ledge, or shore platform, sometimes developing boulder beaches (Kennedy, 2015; Kennedy et al., 2014; Paris et al., 2011; Quartau et al., 2010). At most volcanic islands, lava flows often reach the coastline, spilling over cliffs and filling the shore platforms, facilitating the progradation of lava deltas and potentially increasing the submarine slope instability (Bosman et al., 2014; Di Traglia et al., 2018, 2022; Lipman and Moore, 1996; Ramalho et al., 2013). Lava deltas represent a significant hazard, especially on populated ocean island volcanoes (Poland and Orr, 2014). The detailed characterization of these lava-fed deltas provides information of great interest for different purposes, among which we can point out coastal, volcanic, and paleo-environmental studies (e.g., Perez-Torrado et al., 2015; Quartau et al., 2015; Smellie et al., 2013; Soule et al., 2021; Zhao et al., 2020).

On the other hand, the relevance of wind-generated waves and tides to the development of coastal cliffs has long been recognized as an essential contributor to long-term coastline evolution (Bird, 2008; Sunamura, 1992). In general, geomorphological erosion processes result from a fluid-structure interaction phenomenon. The fluid medium brings into play the energy it transports to work on the structures it impacts, causing their erosion. In particular, wind-generated waves are the most important erosive agent along most coasts, but their effectiveness varies with wave energy, coastal degree of exposure to their attack, tidal range, and with the nature of the material exposed to wave attack, among others (Ramalho et al., 2013; Trenhaile and Kanyaya, 2007).

Although there is no interruption between the subaerial and the submarine parts when lava flows enter the sea, it is not always possible to reconcile land and offshore data consistently, primarily due to the difficulty of accessing seamless topography-bathymetry data sets (Quartau et al., 2014, 2015). Otherwise, most studies focus on the deeper parts of volcanic islands. They are challenging to carry out because they are dangerous and time-consuming. Moreover, studies with integrated subaerial and submarine data are usually performed at the island scale (e.g., Llanes et al., 2009; Masson et al., 2008; Quartau et al., 2014, 2015), not at a scale of the volcanic edifice. Consequently, little is known about the platform-forming eruptions surrounding these islands.

Understanding these shore subaerial-submarine aggradational-degradational systems provides valuable insights into the relationships between the volcanological evolution of the islands and their coastal landscape development over time (Glass et al., 2007; Quartau et al., 2014, 2015; Zhao et al., 2019, 2020). In addition, when radiometric dates are unavailable, shore platforms can provide relative chronological constraints to estimate the timing of posterosional volcanism (Carracedo et al., 2001; Quartau et al., 2014, 2015). Knowledge of the development of shore platforms is necessary for coastal planning purposes and the assessment of geologic hazards (Zhao et al., 2020), as demonstrated during the 2021 eruption on La Palma Island (Vega et al., 2021).

The Canary Islands lie outside reef-forming seas and are a natural laboratory to study the effects of volcanism, flank collapses, and marine action without attenuation by surrounding coral reefs. Some boundary conditions of these islands can be extrapolated to other ocean volcanic islands as, for example, the absence of coral reefs, the type of tide (mainly semidiurnal with tidal ranges between 1.5 and 3.5 m), the significant differences between windward and leeward shores of islands (with a wetter exposed side and a drier rain-shadow side, and the geology (dominated by ocean island basalts or OIBs) (Gómez et al., 2015; Jeffery and Gertisser, 2018).

This work aims to analyze this volcanic rocky coast setting at the island scale and to assess the constructional and erosive degradational effects on the coast at the scale of one volcanic edifice. The spatial scale ranges from hundreds of meters to kilometers, so it can be considered a macro-scale, according to Gómez-Pazo et al. (2021). We analyze El Hierro Island's rocky coast and the Montaña del Tesoro eruption case study, a Holocene Strombolian basaltic volcanic event that produced a scoria cone, pyroclastic fall deposits, and a lava flow that reached the coastline forming a delta. It exemplifies lava flowing in a subaerial-submarine system with decisive wave action. The availability of detailed (1 m contour line equidistance) bathymetric data (Dirección General de Costas, 2003) allows the connection between subaerial and submarine volcanic morphometry. We integrate field-based observations with topographic and bathymetric data to reconstruct the pre- and post-eruption digital elevation models (DEMs) and, comparing with present-day DEM, to analyze morphometrically the subaerial and submarine impacts of the eruption. The Montaña del Tesoro eruption provides a further analogue for analyzing coastal evolution in emergent volcanic ocean islands.

2. Regional setting / study area

2.1. Geographical and geological setting

The study area is El Hierro Island, Canary Islands, Spain (Fig. 1a and b). The Canaries Archipelago, consisting of a roughly linear 500 km long east-west aligned chain of seven main islands and several islets, is located about 100 km off the NW African coast, between 29°25′ and 27°37′N and 18°10′ and 13°20′W (Fig. 1a), and it is part of the Macaronesian region. The archipelago's total land area is about 7446.95 km^2, where 2,175,952 people lived in 2020 (ISTAC, 2021). The largest island is Tenerife, with 2034.38 km^2 (928,604 inhabitants in 2020), and the smallest is El Hierro, where 11,147 inhabitants lived in 2020 on a surface of 268.71 km^2 (ISTAC, 2021).

This archipelago developed in a geodynamic setting characterized by a thick, rigid, and old oceanic lithosphere (Jurassic, 156 Ma) (Roeser, 1982; Roest et al., 1992) lying close to a passive continental margin and on a slow-moving plate (the African plate) (Negredo et al., 2022). The volcanic activity is associated with a hotspot (Carracedo, 1999; Carracedo et al., 1998; Negredo et al., 2022), such as the Hawaiian Islands (e. g., Sun et al., 2021), Galapagos Islands (Hoernle et al., 2004), the Cabo Verde Islands (e.g., Ancochea et al., 2010, 2012; Ramalho et al., 2010), or La Reunion Island (Lénat et al., 2009). This activity probably started in the late Cretaceous–early Miocene and extended into the Holocene, generating the Canary Volcanic Province (CVP), an ~800-km-long and ~400-km-wide volcanic belt. The spatial and chronological evolution of the Canarian volcanism, from east to west, is due to the progression of the cold, thick, rigid, and slow-moving (~2 cm/y) African plate (Silver et al., 1998) over a mantle plume (e.g., Carracedo, 1999; Geldmacher et al., 2005; Holik et al., 1991; Zaczek et al., 2015) (Fig. 1a). Historical eruptions are unknown only on La Gomera, Gran Canaria, and Fuerteventura islands (Longpré and Felpeto, 2021). Like other intra-plate hotspot volcanic islands (e.g., Hawaii, Cape Verde), the Canary Islands also display the hotspot volcanic stages of evolution: juvenile (shield) stage, volcanic quiescence stage, and rejuvenated stage. The easternmost islands (Fuerteventura and Lanzarote) are in the rejuvenated stage, where the erosive processes play a significant role, while the westernmost ones (El Hierro and La Palma) are in the juvenile stage, which is characterized by high eruption rates and fast volcanic growth
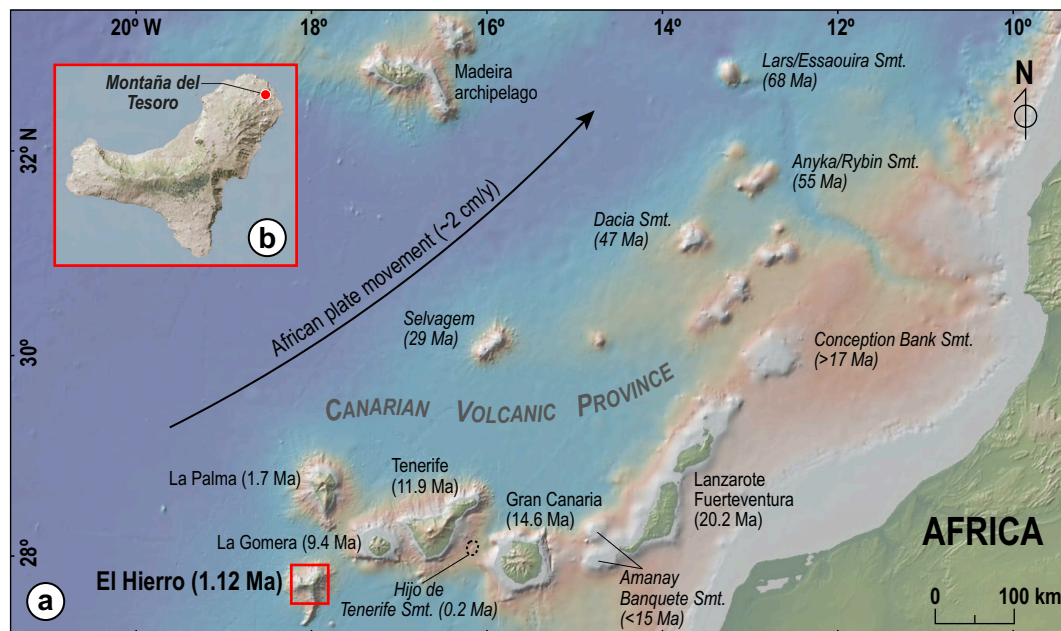
Fig. 1. Regional setting of El Hierro in the volcanic province of Canary Islands (a) (Geldmacher et al., 2005; Guillou et al., 2004; Ryan et al., 2009), and location of the Montaña del Tesoro in El Hierro Island (b).

(Carracedo et al., 2001).

El Hierro Island is the most southwesterly (Fig. 1) and youngest of the Canary Islands, with the oldest subaerial rocks dated at 1.12 Ma (Guillou et al., 1996). It is the emergent summit of a volcanic shield that rises from ~4000 m deep seafloor to 1502 m above sea level at the island's center (*Pico Malpaso*). The estimated volume (subaerial and submarine) of El Hierro reaches from 3200 km^3 (Benito-Saz et al., 2019) to 5500 km^3 (Schmincke and Sumita, 2010). However, considering the palaeosurface supporting the island is irregular and not a plane, the volume estimates reach 6065 km^3. The most characteristic feature of El Hierro is its tetrahedron shape, with edges formed by three convergent volcanic ridges (rift zones) at 120° and separated by wide embayments (Carracedo, 1994; Gee et al., 2001a) (Fig. 2a). The three-armed rift system controls the present-day structure, morphology, and recent volcanic eruptions of El Hierro (e.g., Acosta et al., 2005; Carracedo, 1994, 1996, 1999). This triple-armed shape of El Hierro is further enhanced by the scars of several giant gravitational landslides that truncated all three flanks and removed ~10 % of its total volume (Carracedo et al., 2001; Gee et al., 2001a, 2001b).

The subaerial development of the island resulted from the overlapping growth of three principal volcanic edifices: (1) Tiñor Volcano (1.12–0.88 Ma), (2) El Golfo Volcano (545–176 ka), and (3) the recent rift volcanism (<158 ka) (Becerril et al., 2013, 2014, 2016; Carracedo et al., 2001; Guillou et al., 1996). Their rapid and unstable growth turns out to be one of the conditioning factors for the occurrence of the five giant gravitational landslides identified at El Hierro: Tiñor (<880 ka), (2) Las Playas I (545–176 ka), and II (176–145 ka), (3) El Julan (>158 ka), (4) El Golfo (133–21 ka) and (5) Punta del Norte (unknown age) (Carracedo, 1999; Carracedo et al., 2001; Longpré et al., 2011; Masson, 1996; Masson et al., 2002; Urgeles et al., 1997; Watts and Masson, 1995). These large-scale landslides (commonly in debris avalanches) are a prominent feature of the Canary Islands (Mitchell et al., 2003). The dissection by fluvial processes is poorly developed on El Hierro Island.

Montaña del Tesoro is a 121 m high cinder cone located at the northeastern rift system within 1.5 km to the capital Valverde and about 2 km to the island's small airport (El Hierro Airport) (Figs. 1b and 2). Together with Montaña de Aguarijo and Montaña Chamuscada, represent the principal platform forming eruptions at the NE rift (Prieto-Torrell et al., 2021). The most distinct feature of the Montaña del Tesoro

eruption is that its lava flow cascades over a paleo-cliff's edge and spreads over a shore platform. The town of Tamaduste is built upon the platform lava of the Montaña del Tesoro eruption (Fig. 2b).

The Montaña del Tesoro eruption was dated at 9 ± 6 ka (± 2σ) BP by the K/Ar radiometric method (Rodriguez-Gonzalez et al., 2012b). Although this method is not very accurate for Holocene eruptions, it confirmed the youth of this volcanic event. Risica et al. (2022) obtained two probable ages by the Palaeosecular Variation (PSV) curve (1205–1041 and 965–941 y BP) and one from charcoal found in the soil below the Montaña del Tesoro's lapilli that yielded a radiometric age of 1080–958 cal AD. These new ages place the Montaña del Tesoro eruption around 1050 years BP.

2.2. Climatic and geomorphic setting

The climate of the Canary Islands is subtropical, moderated by the oceanic Canary Current and prevailing northeast trade winds, and it is conditioned especially by altitude. According to the Köppen-Geiger climate classification, the Canary Islands present hot desert (BWh) and cold desert (BWk), hot steppe (BSh) and cold steppe (BSk), hot and dry summers (Csa), and dry and warm summers (Csb) climates (AEMET, 2012). Geomorphology and altitude determine particular geographic and climatic characteristics for each island. In El Hierro, we find an altitudinal zonation BWh-BSh-BSk-Csb from the coast to the highlands. Annual average air temperature variation ranges from 20 °C at sea level to below 10 °C in the highlands of the Canary Islands, e.g., 12 °C in El Hierro (AEMET, 2012). The precipitation is unevenly distributed due to orographic effects and exposure to the prevailing and persistent northeasterly trade winds. Annual average precipitation varies between 100 and 1000 mm/y for the Canaries Archipelago and 100–800 mm/y for El Hierro.

Erosional landforms prevail in the general landscape of the easternmost islands of Canaries Archipelago. Instead, the western and younger islands generally exhibit a rugged relief where the principal volcanic forms are well noticeable. The coasts of the Canary Islands show rough cliffs, shore platforms, and basaltic sand and gravel beaches, especially on the older eastern islands.

The coastal landscape of the Earth has been profoundly modified by the gradual sea-level rise caused by the melting of continental ice sheets
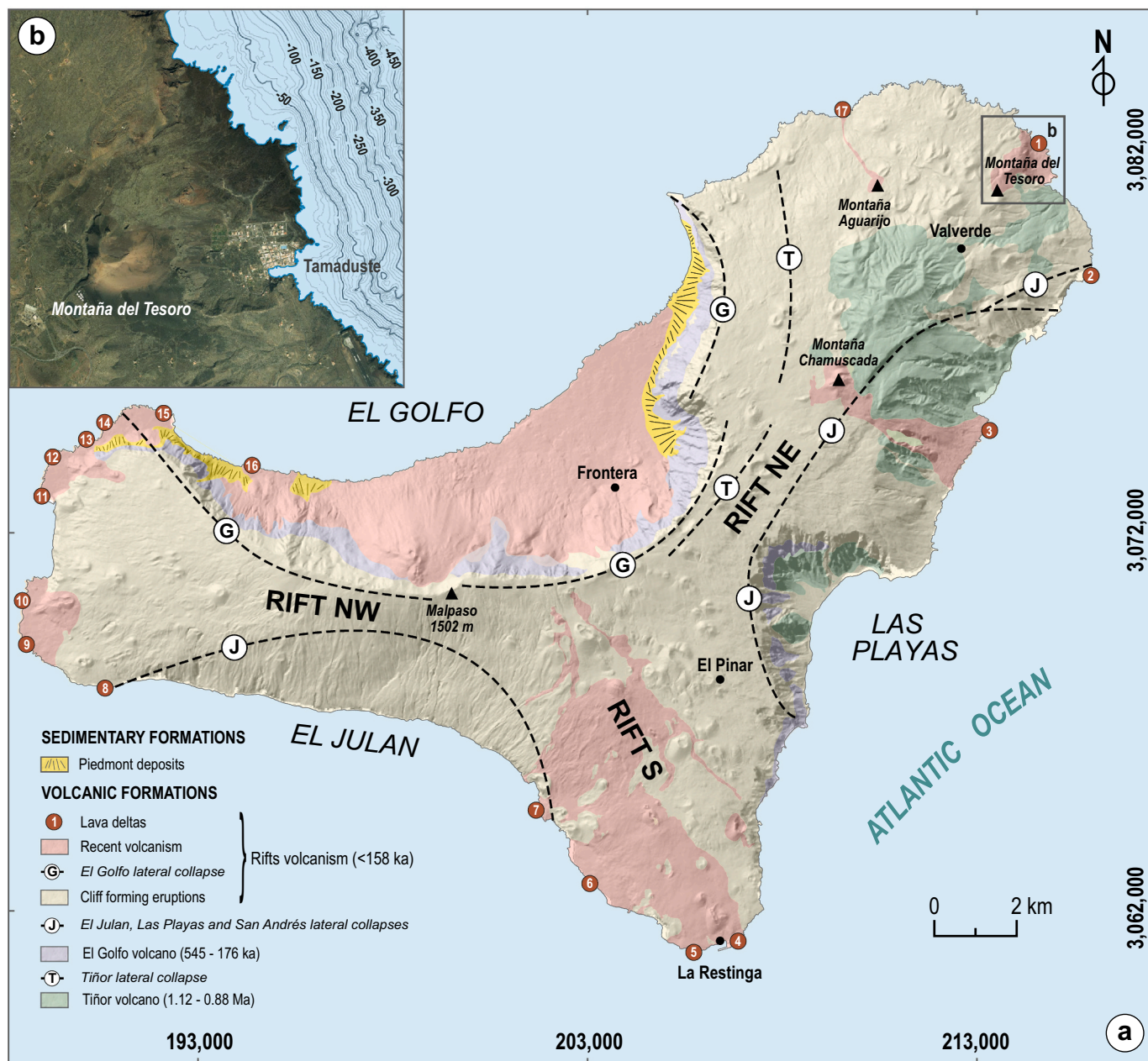
Fig. 2. (a) Simplified subaerial geology of El Hierro Island (Prieto-Torrell et al., 2021), coordinate system WGS84-UTM Zone 28 N (EPSG: 32628). The lava deltas identified in the contemporary shore platform are indicated (see Table 3 for details). (b) Satellite image of the study area showing shore platform bathymetry (Cartográfica de Canarias GRAFCAN, 2021).

since the Last Glacial Maximum (LGM), about 20,000 years ago (Lambeck et al., 2014; Osman et al., 2021). The post-LGM marine transgression has been recorded in the Canaries' coasts by migration of marine erosion towards inland, forming shore platforms (Carracedo et al., 2001; Rijsdijk et al., 2013). Carracedo et al. (2001) observed as lavas forming cliffs had ages older than about 20 ka, while those forming coastal platforms yielded younger ages. This fact was used for the relative dating of volcanic eruptions that reach the coast, distinguishing the pre- and post-LGM eruptions.

The young relief of El Hierro presents steeply plunging cliffs that are associated with laterally eroded cones and lava flows. In addition, there are shore platforms that record the past climate changes on sea level variations which, in turn, have been covered by lava flows. This complex scenario is captured in the eruption of Montaña del Tesoro (Fig. 2).

2.3. Meteoceanic setting

Due to its geographical location, the Canaries are within the fairly regular Trade Winds belt on the southern edge of the Azores High. The trade winds regime exhibits a clear seasonal pattern throughout the year, mainly governed by the relative intensity and location of the Icelandic Low and Azores High-pressure systems. During summer, trade winds blow with moderate or weak intensity from the N-NNE directional sector with frequencies between 90 % and 95 %, while in winter, its intensity decreases significantly, and its frequency is reduced to about 50 %. The weakening of the Azores high-pressure system during the winter allows for the sporadic arrival of some storms, mainly from the North-Northwest Atlantic sector. Spring and autumn represent transitional periods between these situations (Guerra-Medina and Rodríguez, 2021; Pérez et al., 2014).

Wave climate in the archipelago is naturally related to atmospheric conditions, and consequently, average wave conditions are relatively mild, especially during the period when trade winds prevail. However, the approach of low-pressure atmospheric systems from the northern part of the Atlantic, the passage of atmospheric storms, or even some episodic extratropical storms close to the islands, generally traveling towards the eastern coasts of the northern North Atlantic, can lead to the generation of moderate or severe wave conditions. However, severe wave conditions on the archipelago's exposed coast are often swell waves irradiated from more or less distant storms (Chiri et al., 2013). This is the reason why the Canary Archipelago belongs to the class of swell-dominated coasts (Davies, 1980; Semedo et al., 2011).

In addition to meteorological conditions, a proper understanding of the wave conditions in the archipelago requires bearing in mind other aspects related to its distance from the African continent and its complex geometric configuration. The short distance between the African coast and the easternmost islands considerably limits the development of wave fields approaching the islands from the east. On the other hand, due to the relative position of each island within the archipelago, the northern and western flanks of the archipelago are the most exposed to wave action while acting as a protective barrier for the opposite faces and the islands in the shaded areas generated by them. Another important feature in this respect is the existence of deep channels between some islands, which allows the propagation along the main axis of such channels for wave fields arriving from that direction to a given coastal stretch (Guerra-Medina and Rodríguez, 2021). In brief, average wave conditions are mild but with significant local variations due to the sheltering effects among islands and the orientation of the different coastal stretches (degree of exposure) (Di Paola et al., 2020).

Regarding tidal conditions, the tidal regime in the Canary Islands is microtidal, with a semidiurnal tide pattern and a tidal range oscillating approximately between 0.5 m and 3 m, and a mean value close to 1.5 m. Furthermore, meteorological residuals are almost negligible, ranging between ±20 cm approximately, but with a modal value nearly null (Guerra-Medina and Rodríguez, 2021).

3. Methods

3.1. Rock coast assessment

Coast morphology was analyzed through profiles around El Hierro Island. We surveyed cross-sections based on the Digital Elevation Model (DEM) made from the LIDAR point clouds of the second coverage with a mesh pitch of 2 m (Instituto Geográfico Nacional, 2015) and 1:1000 multibeam swath (sonar) bathymetric (Dirección General de Costas, 2003) digital maps (5 m and 1 m contour line equidistance, respectively). Then, we decided to segment the platform width arbitrarily into two classes, <25 m and > 25 m wide, considering the width as the distance between the coastline (sea level or 0 m) and the bathymetric curve of −1 m. This segmentation was performed using QGIS to assess the development of the insular shelves. In addition, we explored the occurrence of lava flows affecting the shore platform that clearly modified the previous bathymetry.

3.2. Wave climate and tides

Datasets used to characterize wave climate and tidal regime in the study area include wave data obtained from the coupling of wind and numerical wave models, as well as seawater level information, recorded using a tidal gauge, and have been provided by the Spanish Port Authority (Puertos del Estado).

The reanalysis database containing wave information through wind and numerical wave models is called SIMAR and provides information covering 64 years, from January 1958 to March 2022. The location of the selected computational grid node is indicated in Fig. 7. This node is located close to Montaña del Tesoro and exposed to wave conditions

similar to those reaching the study area. In particular, the wave data set includes hourly values of spectral significant wave height, H_{m0}, peak period, T_p, and mean wave direction, D_m. The frequency of occurrence of different wave conditions has been examined by elaborating empirical joint distributions of H_{m0} and D_m, as well as T_p and D_m, displayed in polar coordinates (wave rose) to facilitate their interpretation.

Wave energy flux, or wave power, by unit of wavefront, has been computed as $P = C\, T_e\, H_{m0}^2$, where T_e is the wave energy period and has been obtained by assuming a Pierson-Moskowitz spectrum so that $T_e = 0.86\, T_p$. The constant C equals 0.49, which includes sea water density and acceleration of gravity (e.g., Chiri et al., 2013). Directionality and the timing of occurrence of the most severe wave conditions during each year have been identified and shown as polar plots, including information on the associated significant wave height and peak period (Fig. 8).

Experimental measurements of sea level were obtained from the tide gauge network (REDMAR) of Puertos del Estado and consist of hourly values of the sea water level covering the period from May 2004 until March 2022 at La Estaca Harbor (Fig. 7). The tidal gauge used from 2004 to November 2009 was a pressure sensor; from then until today, it has been a radar-type sensor. It is interesting to note that with a series of this length, nearly 18 years, the nodal cycle of the Moon, 18.6 years, is almost wholly included, thus covering all amplitudes and phases of the astronomical tide.

Seawater level observations indicate the height of the sea surface above the tidal datum. They may be understood as the combination of two components: the astronomical tide due to the time-varying gravitational attraction of the Moon and Sun, and the meteorological residue, or perturbation of the sea level elevation caused by meteorological conditions. Harmonic analysis of sea level measurements allows to separate both contributions (e.g., Rodríguez et al., 1999). The representative statistical parameters were derived once the empirical probabilistic distribution of sea water level, astronomical tides, and meteorological residues were obtained.

3.3. Fieldwork mapping

The geological mapping of the Montaña del Tesoro eruption, and the reconstruction of the geomorphology and topography before and after this volcanic event, required intensive and meticulous fieldwork. This fieldwork identified and analyzed the volcanic landforms, i.e., the cone, the lava flow and its levées, the pyroclastic fall deposits, and the underlying relief (Rodriguez-Gonzalez et al., 2010, 2012a). The geological mapping of these units was carried out with a tablet (iPad Pro 11 Wi-Fi + cellular model + GPS / GNSS receiver) that allows digitizing with a pencil device the contact lines and geolocation points (photos, sketches, samples, etc.) by using the FieldMove application (Fig. 3). We use high-resolution raster maps (e.g., orthophoto, LIDAR, topography), as MBtiles files (512 × 512 tile size and 16 Zoom Levels), as a reference (base) layer for this application. Since the new vector elements are displayed on the reference map, we can visually verify the accuracy as we map. The vector data structure allows geologic data to be represented in a single vector object, making it easy to digitize and store large and complex map data. Subsequently, we can separate the data into different thematic layers (e.g., unit contacts, outcropping structures, or individualized eruptions), gaining flexibility in designing the maps of interest. Finally, the acquired data is exported to a KMZ file and entered into a Geographical Information System (GIS) environment to accurately estimate the required morphological parameters and derivates, such as eruption output volume, slope, and terrain aspect (Fig. 3).

3.4. Paleogeomorphological reconstruction

Remotely Operated Vehicle (ROV) images or geophysical profiles have not been available for detailed observations of submarine landforms. However, the 1:1000 multibeam swath (sonar) bathymetry (Dirección General de Costas, 2003) permitted the reconstruction of the
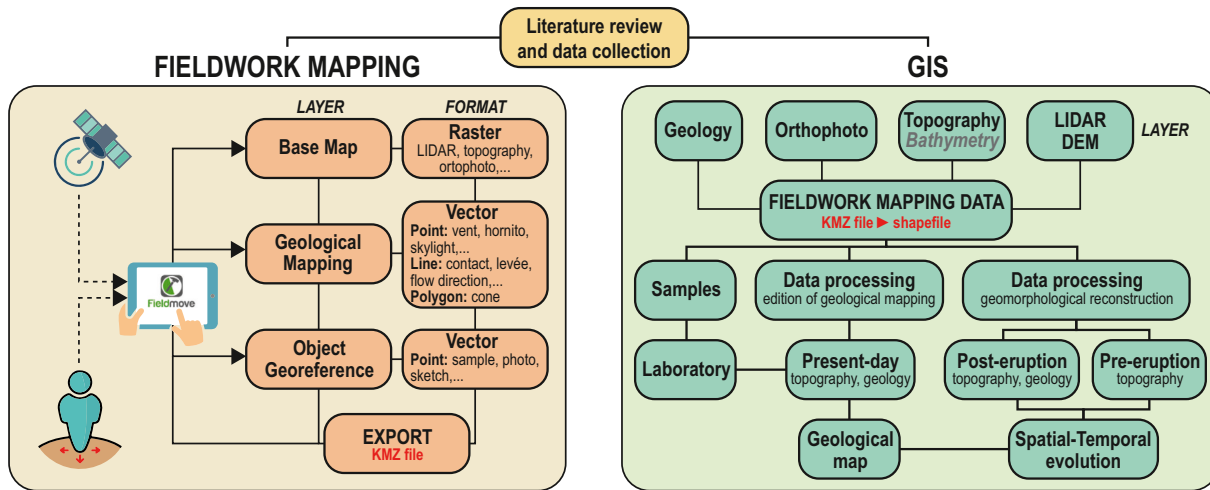
Fig. 3. The conceptual flowchart shows the fieldwork mapping and Geographical Information System (GIS) study methodology.

submarine lava flows and their front. For the paleogeomorphological reconstruction, field-derived data were combined with the available 1:5000 topographic (Cartográfica de Canarias GRAFCAN, 2006) and the before-mentioned bathymetric digital maps (5 m and 1 m contour line equidistance, respectively) to modify by hand the present-day contour maps and derive the pre- and post-eruption relief. The pre-eruptive submarine terrain is reconstructed by observing the slope break produced by the lavas over the platform on the bathymetric contours. The post-eruption landscape is reconstructed from the visible lava thicknesses along the current coastline, the arrangement of their erosional remnants, and the bathymetric contours' morphology. We assume for this modeling the current sea level in the pre- and post-eruption evolutive stages for these reconstructions and a negligible degradation in distal submerged lava fronts.

Three coastlines are recognized (pre- and post-eruption and current coastline; CL_1, CL_2, and CL_3, respectively) (Fig. 4). The post-eruption and current coastlines reflect the lava flow foreparts that gained land from the sea (CL_2) and then retreat due to marine erosion (CL_3) (Fig. 4). Modifications of present topographic and bathymetric contour lines and the derivate Digital Elevation Models (DEMs) were processed using TNTGis 2020 software (Microimages Inc.). The pre- and post-eruption DEMs were produced with a cell resolution of 5×5 m using the minimum curvature method as the interpolation algorithm that continuously compares the results with the current DEM (Rodriguez-Gonzalez et al., 2010). Terrain slopes were determined from the DEMs, computed with sufficient smoothing, and using a differential geometry approach based on the weighted averages of all points within the 3×3 neighborhood (Warren et al., 2004). The comparison between the pre- and post-eruption DEMs and the present-day DEM allows us to identify the geomorphological evolution of the study area and perform the morphometric analysis.

3.5. Morphometric modeling

The DEMs allowed the calculation of several morphometric parameters related to the cone, lava flows, pyroclastic sheet-like fall deposits, and basement (Rodriguez-Gonzalez et al., 2010, 2011, 2012a). We apply a cut-and-fill analysis process for volume estimates to the three DEMs obtained (pre-eruption, post-eruption, and present-day). This process compares two raster surfaces of the same area and identifies locations where their elevation values differ.

The total original volumes of the eruption (V_{TE}) and the cone (V_{CE}) are obtained from the difference between the post-eruption and pre-eruption DEMs. For volume estimates of pyroclastic sheet-like fall deposits, we determine an average volume based on the minimum distal

and maximum proximal thicknesses for post-eruption (V_{PE}) and present-day (V_P) stages. This method is used due to the minimal changes that their low thicknesses introduce in the landscape at the more detailed work scale (1:1000) (Rodriguez-Gonzalez et al., 2012a).

The complexity of the landforms configuring the lava flows is a challenge that needs another strategy. The lava flow field was discretized according to the coastline evolution and lava front sectors and their subaerial or submarine placement (Fig. 4). In this way, Sector 1 includes the area from vent to pre-eruption coastline CL_1; Sector 2, the area from pre-eruption (CL_1) to current (CL_3) coastlines; Sector 3, the area from current (CL_3) to post-eruption (CL_2) coastlines; and Sector 4 represents the area from the post-eruption coastline (CL_2) to submarine lava flow front. The resulting partial lava flow volumes and areas were used for the morphometric analysis of the post-eruption and present-day stages (Table 1). They were the basis for determining any other volumes and derivates of interest.

Total post-eruption lava flows volume (V_{LE}) is the sum of subaerial and submerged volumes (Fig. 4), being

V_{LE} = subaerial volume [$V_{L1E} + V_{L2E} + V_{L3E}$] + submerged volume [$V_{L2sE} + V_{L3sE} + V_{L4sE}$] (Fig. 4c).

For degradation (Fig. 4), the volume eroded by fluvial action (V_{Lef}) is estimated from

V_{Lef} = denuded subaerial volume in Sector 1 ($V_{L1E} - V_{L1}$) + denuded submerged volume in Sector 2 ($V_{L2E} - V_{L2}$) (Fig. 4a, d);

and the volume eroded by marine action (V_{Lem}) is

V_{Lem} = denuded subaerial volume in Sector 3 ($V_{L3E} - V_{L3}$) + denuded submerged volume in Sector 3 ($V_{L3sE} - V_{L3s}$) (Fig. 4d).

The V_{L2sE} and V_{L2s} are the same in Sector 2 because they are protected by subaerial lava and configure the current cliff on the coast. The volume values are also the same for V_{L4sE} and V_{L4s} because there is no wave action; therefore, it does not present erosion and maintains the original morphology.

If not explicitly stated, all volume estimates are expressed as bulk erupted volume, including the solid and void volumes of the different volcanic units, without dense rock equivalent (DRE) corrections. For DRE volumes, correction factors assume (e.g., Rodriguez-Gonzalez et al., 2010) a porous volume fraction of 75 % for the volcanic cone (Mangan and Cashman, 1996) and 25 % for basaltic a'a' lava flow (Wolfe, 1988).

4. Results

4.1. El Hierro shoreline

The coastal landscape of El Hierro Island is dominated by stacks of lava flows (Fig. 5a), but also there are some spectacular sections of
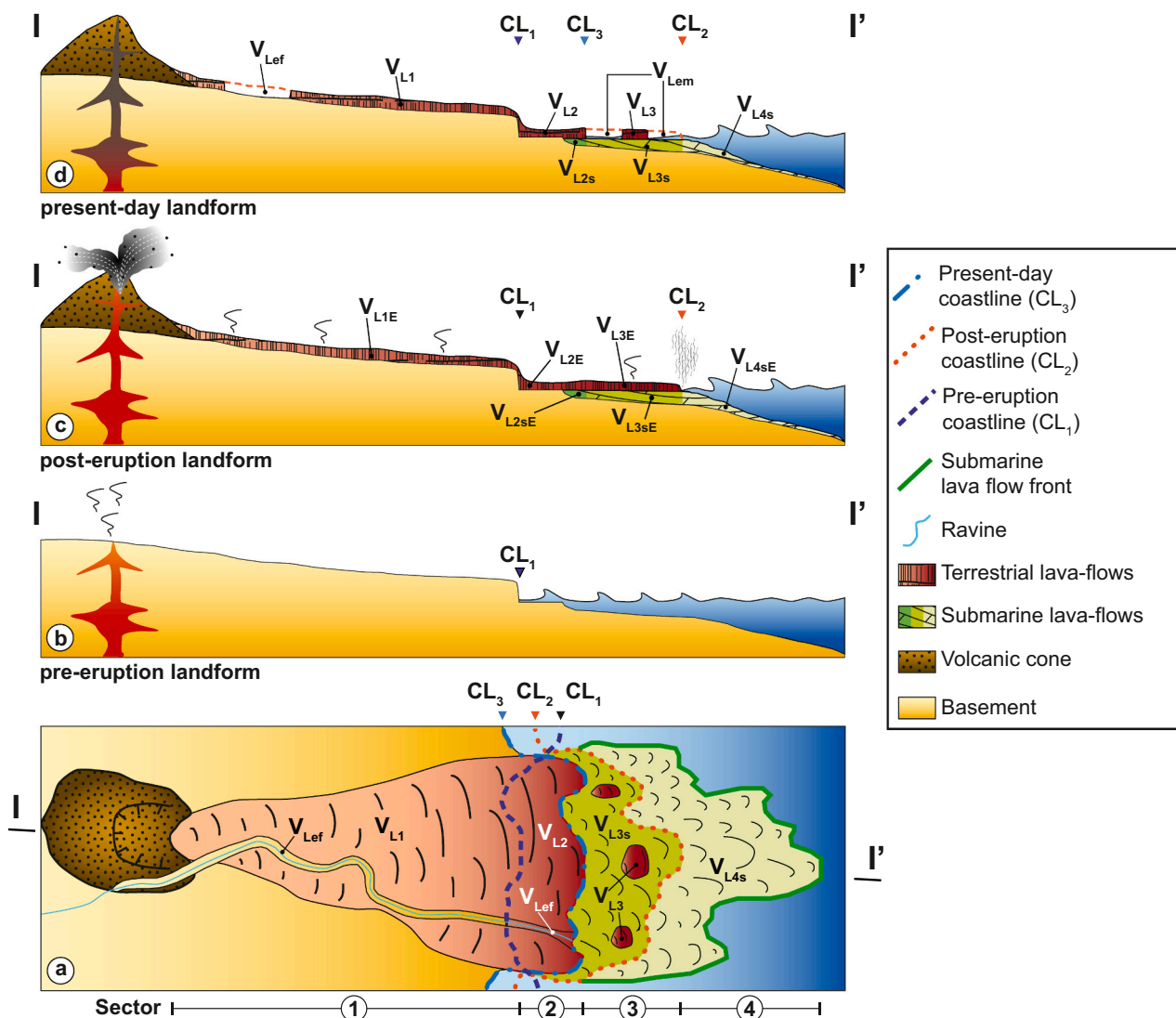
Fig. 4. (a) Simplified geological sketch map of the Montaña del Tesoro eruption. (b-d) Cross-sections of the pre-, post-, and present-day evolutive stages. Three coastlines are recognized (pre- and post-eruption and current coastline; CL_1, CL_2, and CL_3, respectively). The lava flow field was sectorized to facilitate the study: Sector 1 includes from the vent to the pre-eruption coastline (CL_1); Sector 2 from the pre-eruption coastline (CL_1) to the current coastline (CL_3); Sector 3 from the present coast (CL_3) to the post-eruption coastline (CL_2); and Sector 4 from the post-eruption coastline (CL_2) to the lava flow front. See the text for an explanation of the different volumes (V).

Table 1

Partial lava flow volumes are discretized according to the coastline evolution, lava front sectors, and their subaerial or submarine placement. This discretization is used for the present-day (PrD column) and post-eruption (PtE column) stages of landscape evolution.

|	Sector 1 from vent to pre-eruption coastline (CL_1)		Sector 2 from pre-eruption (CL_1) to current (CL_3) coastlines		Sector 3 from current (CL_3) to post-eruption (CL_2) coastlines		Sector 4 from post-eruption coastline (CL_2) to submarine lava flow front	
	PrD	PtE	PrD	PtE	PrD	PtE	PrD	PtE
Terrestrial	V_{L1}	V_{L1E}	V_{L2}	V_{L2E}	V_{L3}	V_{L3E}	–	–
Submerged	–	–	V_{L2s}	V_{L2sE}	V_{L3s}	V_{L3sE}	V_{L4s}	V_{L4sE}
Erosion	V_{Lef}		V_{Lef}		V_{Lem}		–	

volcanic cones (Fig. 5b), both forming steep cliffs. Cliff morphology varies around the island, from plunging cliffs to shore platforms with arches (Fig. 5c and d), sea stacks, blowholes, and sea caves. It is

noteworthy the practical absence of beaches.

Concerning the shore shelves, the <25 m wide platforms represent 65.6 % of the coastline (87.6 km), while 34.4 % consists of >25 m wide platforms (45.9 km). The maximum continuous length is 11.0 km in the first case, and the minimum is 0.3 km ($n = 32$ segments). For the >25 m wide platforms, the maximum continuum length is 6.0 km and the minimum 0.2 km ($n = 32$ segments). The >25 m wide platforms lie mainly in the northern and western areas of the island (Fig. 6).

The study area is affected by predominant winds coming from the NNE direction, corresponding to the persistent trade winds, blowing with moderate or weak intensity and impinging almost perpendicular to Montaña del Tesoro coastal stretch, mainly during summer.

The occurrence of wind-generated surface gravity waves evidences the strong atmosphere-ocean coupling resulting from the exchange of energy and momentum at the sea surface interface. The energetic content of a wave field grows with the wind speed, the duration of the period during which wind transfers energy and momentum to the sea surface, and the extension of the surface over which these fluxes take place, known as fetch. The sea surface exhibits a complex and random
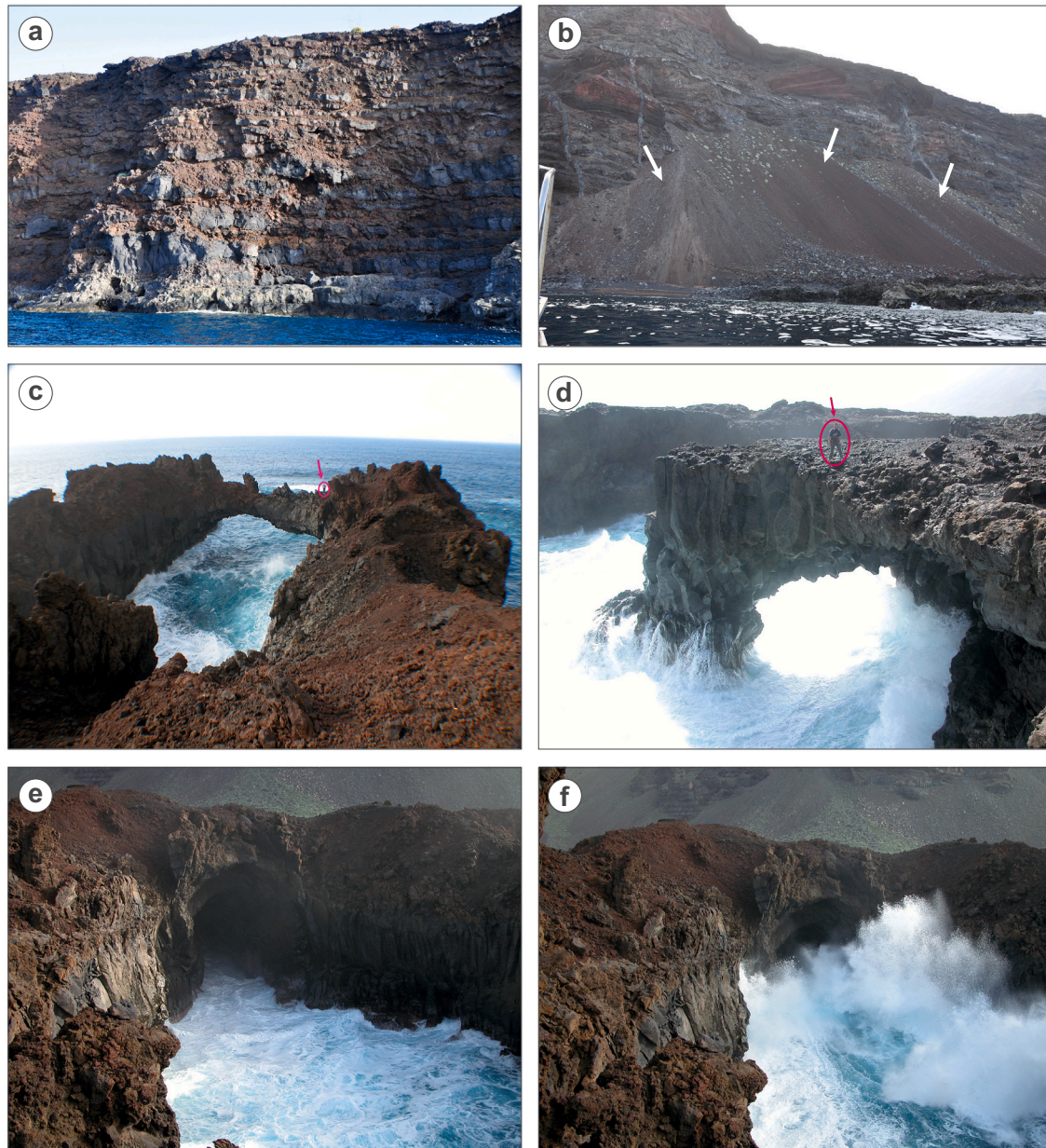
Fig. 5. Characteristic coastal landforms of El Hierro Island. (a) Plunging cliff on stacks of lava flows on the coast of the Mar de las Calmas. (b) Cliff on a volcanic cone on the coast of the Mar de las Calmas; note a large amount of debris at its base (white arrows). (c) The Puntas de Guitérrez Arch cut in young basalt flows on the NW rift (near profile 1 in Fig. 6) (red arrow indicates a person as scale). (d) The Punta de la Sal Arch cut in old basalt flows on the NE rift (near profile 1 in Fig. 6) (red arrow indicates a person as scale). (e-f) Effect of wave attack on a lava tube from Puntas de Gutiérrez. (For interpretation of the references to colour in this figure legend, the reader is referred to the web version of this article.)

structure within this area, and wave fields are known as wind seas. As waves travel out of the fetch across the ocean basins, they undergo significant transformations giving rise to wave fields, referred as swell waves, that progressively reduce their chaotic aspect while retaining their random nature, with significant wave height decreasing and peak periods increasing with the distance from the fetch. A standard approach is to distinguish between the two types of waves according to whether the peak period value is less or >10 s (e.g., Goda, 2010).

Inspection of the wave rose for significant wave heights, produced with the hourly data for the reanalysis point shown in Fig. 7a for the period between January 1958 and March 2022, reveals the existence of two main wave directions of wave approach to the northeast coastal flank. The prevailing (most frequent) direction is identified along the longitudinal axis of the channel between the islands of La Palma and La Gomera, in an approximately NNE direction. Waves arriving from this narrow sector are mild, with heights rarely reaching 4 m. On the contrary, the dominant (most severe) directional sector presents a higher directional dispersion, covering roughly the NW-N circular range but mainly centered on the NW-NNW subsector. Wave fields from this sector are associated with sporadic storms reaching the western side of the island, particularly during winter, but mainly with remote storms located to the north-northwest of the Atlantic at a considerable distance from the islands, giving rise to situations in which significant wave heights of >3 m are relatively frequent and reaching extreme values around 8 m.

Regarding spectral peak periods in El Hierro, periods associated with wave conditions from the prevailing directional sector are often lower than 10 s (Fig. 7b), reflecting the predominance of wind waves.
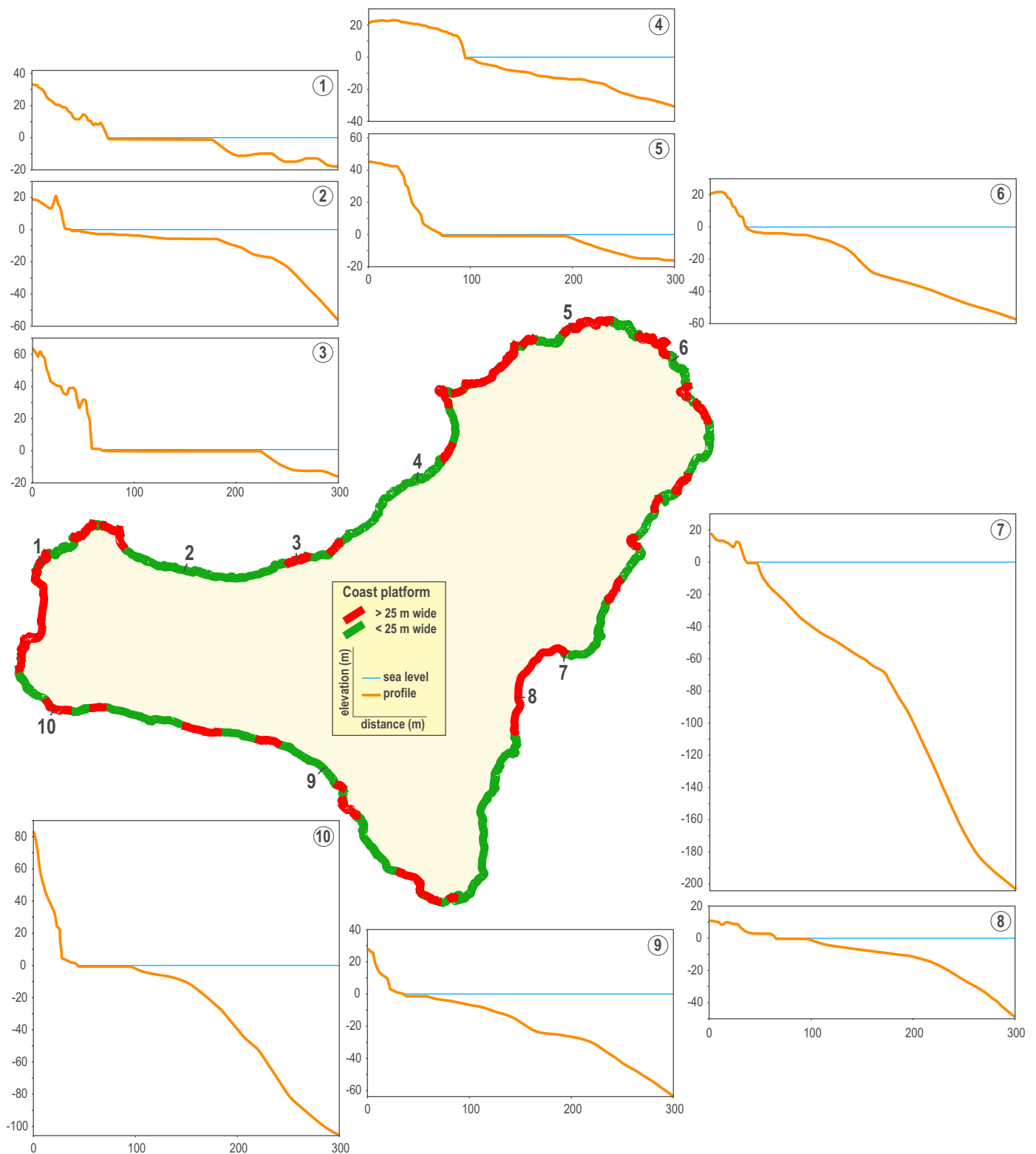
Fig. 6. Distribution of areas with <25 and > 25 m wide shore platforms on the coastline of El Hierro Island. Profiles 1–10 represent typical sections of the coast, mainly consisting of stacks of lava flows, projected to uniform height and distance. The most extensive platforms (>25 m wide) correspond to the highest active marine erosion (profiles 1, 3, 5, 8, and 10), whereas the narrowest platforms (<25 m) lie in the areas where the wave attack is more attenuated (profiles 2, 4, 6, 7, and 9).

However, periods have a frequency higher than 10 s in the dominant sector, reaching values higher than 20 s, showing the predominance of swell conditions, as it corresponds to an area with the preponderance of westerly swell.

Concerning the variation of wave conditions around the island, it has been observed that wave energy flux, or wave power, is higher along the western edge of the island, which is exposed to storms approaching from the North Atlantic and to swell arriving from more or less distant storms,
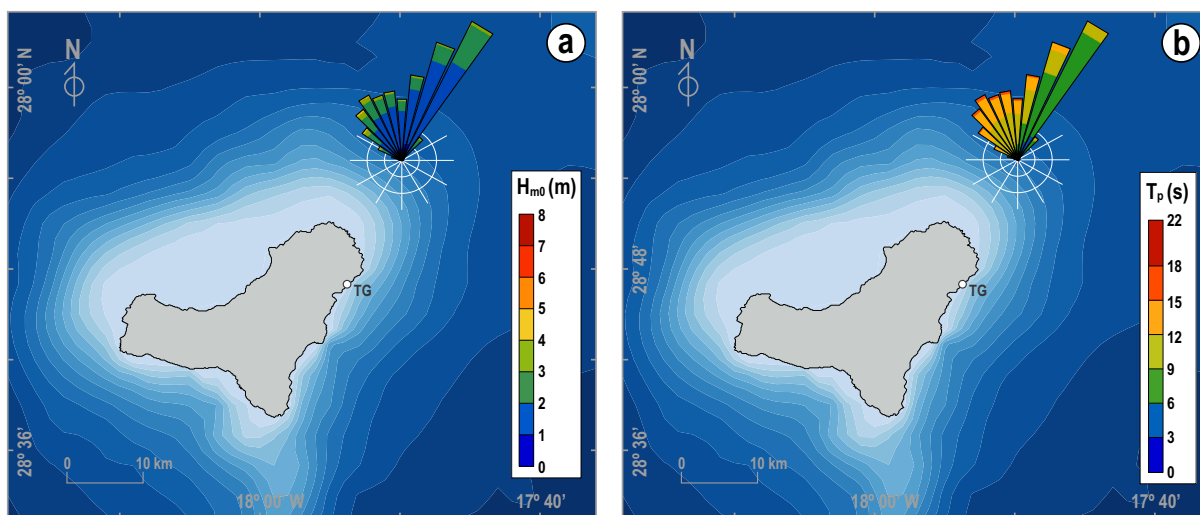
Fig. 7. Significant wave height or H_{m0} (a) and peak wave period or T_p (b) roses for hourly values, at a selected computational node offshore Montaña del Tesoro, for the period 01/1958–03/2022. TG, tidal gauge at La Estaca Harbor.

while the contribution of the trade winds virtually disappears in this side (Chiri et al., 2013; Iglesias and Carballo, 2011). On the opposite flank, this contribution remains the only one while the wave action on the coast is substantially lower due to the sheltering effect generated by the island against the NW storms. Due to the orientation and geometric configuration of the island, the SW coast of the island represents a shadow zone, protected from the action of both types of wave fields, thus receiving the name "Sea of Calms" (*Mar de las Calmas*).

Bearing in mind that the erosive potential of waves increases with the amount of energy they carry, wave energy flux, or wave power, was evaluated for the most energetic annual events in terms of the direction of approach to the study area and the period of the year in which they occurred. Fig. 8a depicts wave energy flux in kW/m as a function of the direction of wave propagation during each of the major annual storms. Most energetic storms reach the Montaña del Tesoro area from the WNW-NNW directional sector, mainly from the NW, with wave power ranging between 50 and 460 kW/m. In contrast, stormy events arriving from the prevailing sector are much less frequent and do not exceed 150 kW/m. Regarding the timing of annual maximum storms (Fig. 8b), extreme wave conditions undergo a clear seasonal pattern so that it is possible to distinguish two roughly semi-annual periods, one from

November to May with the most energetic swell conditions, especially in winter, and another from June to October with mild energetic conditions. In short, the wave energy flux towards Montaña del Tesoro occurs in two main directions. Most of the year, low and moderate wave power arrives from a narrow sector centered around the NNE direction, almost perpendicular to that location, whereas more energetic waves, usually long swell, approach sea cliffs obliquely from NW but roughly ranging between WNW and NNW.

Sea cliffs may occur in various tidal environments. In general, the most important aspect of tides in geomorphology is their vertical range, known as the tidal range, and is defined as the difference in level between one high tide and the next low tide. When the average range of tides is lower than 2 m, the coast can is classified as microtidal; for tidal ranges between (2–4 m), the tidal regime is considered as mesotidal, whereas coasts with tidal ranges over 4 m are macrotidal (Pugh and Woodworth, 2014). The tidal range determines the vertical zone over which a wave acts. Where the tide range is small, wave energy is concentrated in a narrow vertical area, and where the tide range is larger, wave energy is more dispersed. Thus, on microtidal coasts, wave energy is concentrated within a narrow vertical zone, facilitating cliff-base erosion. In contrast, on macrotidal coasts, cliffs are reached by
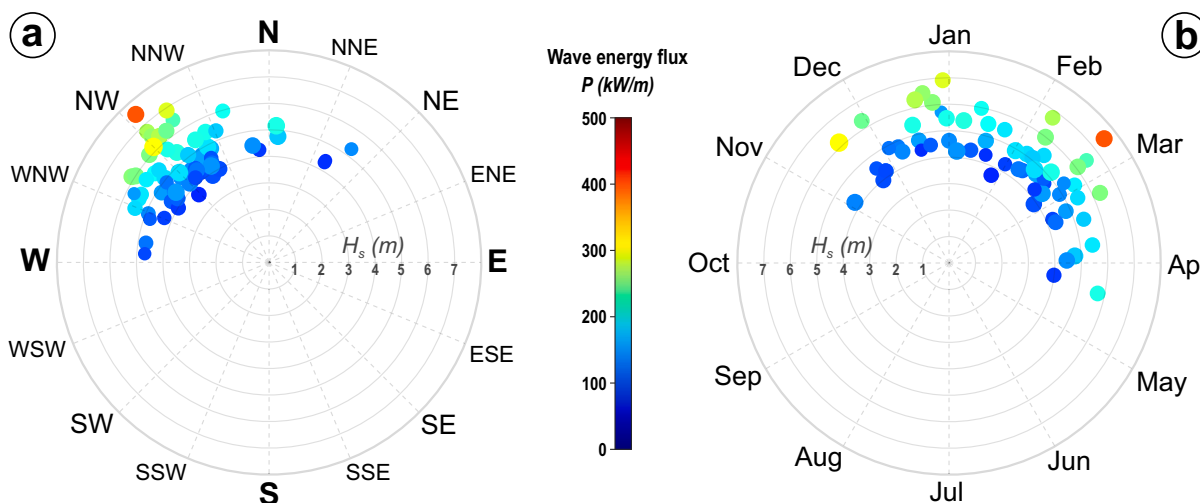

Fig. 8. Wave energy flux associated to annual maximum storms at selected computational node offshore Montaña del Tesoro, for the period 01/1958–03/2022, in terms of approach direction (a) and time of occurrence throughout the year (b).

waves at different vertical levels briefly and intermittently.

On the other hand, the elevation of the sea surface is significant because it determines the degree of energy dissipation experienced by waves before reaching the cliff base by changing the depth of the water column over which they propagate (Trenhaile, 2016). In this sense, it is interesting to consider that additional factors, such as storm surges, may contribute to modifying local sea surface elevation in addition to astronomical tidal fluctuation. The resulting sea level largely controls the height of the wave attack (Sunamura, 2015).

The tidal regime examined using data from a tidal gauge installed at La Estaca Harbor (Table 2) indicates that the tide in El Hierro is microtidal. Consequently, the erosive action of the waves is concentrated in a relatively restricted range of elevations, and it is more frequent at each elevation than in mesotidal and macrotidal regimes, which facilitates the base cliffs erosion. The character of the tidal cycle is semi-diurnal, including two similar but slightly different high and low tides per day and a tidal range oscillating approximately between 0.4 and 2.8 m. The average elevation is close to 1.6 m, and the modal value is around 1.9 m. Furthermore, meteorological residuals (storm surges) are significantly small, ranging between ±20 cm approximately, but with an almost null modal value. This factor is therefore of little importance in determining the level at which the waves act on cliffs.

4.2. Lava deltas

The exploration of the shore platform around the El Hierro showed the occurrence of 17 lava flows that ran below sea level affecting this insular shelf (Fig. 2, Table 3). The vents that originated these lava flows are indicated in Table 3. Fig. 9 illustrates the morphological modifications introduced by some of these lava flows on the bathymetry. The previous bathymetry is altered, and these changes can be used for morphometric analysis of the eruptive event. In this way, we selected the Montaña del Tesoro eruption (Fig. 9b) as a representative case study to integrate subaerial and submarine data at a scale of a volcanic edifice and proceed with the morphometric modeling.

4.3. Morphometric modeling of Montaña del Tesoro eruption

The Montaña del Tesoro eruption developed a main cone that grew on a slightly sloping surface installed on a paleo-cliff's structural roof. At the NE base of the main cone, a small lava shield of scutulum type (Noe-Nygaard, 1968; Walker, 2000) developed from where the emission of all lava flows took place. These flows fanned out towards the edge of the paleo-cliff. Once this was reached, they formed numerous cascades to coalesce at their base. From here, the lava flows spread through a platform until reaching the sea, gaining ground and modifying the coastline. The pyroclastic fall was especially intense to the SE of the cone. The geological map of these units is in Fig. 10. Fig. 11 shows several details of the landforms of the Montaña del Tesoro volcano. The morphometric parameters and their derivatives of the Montaña del

Table 2
Tidal statistics at La Estaca Harbor, El Hierro. Data from Puertos del Estado tidal gauges network (REDMAR). Observational period: May 2004 to March 2022 (hourly values). Tidal gauges: pressure sensor (Aanderaa) from 2004 to November 2009 and Radar MIROS since December 2009. The zero of the tide gauge is the zero of the harbor and is located 4.323 m below the B. M. MARE-HIERRO2 and 1.420 m below the mean sea level in El Hierro. The hydrographic zero is found 3.995 m below said nail.

	Sea water level (cm)	Astronomical tide (cm)	Residue (cm)	Tidal range (cm)
Minimum	30.90	39.40	−19.70	15.30
Maximum	293.70	284.90	18.50	229.80
Mean	156.55	156.97	−0.46	124.56
Median	156.10	156.70	−0.40	125.60
Mode	181.80	188.90	−0.60	138.00

Table 3
Coordinates of lava deltas affect El Hierro island's contemporary shore platform, indicating the respective vents. Fig. 2 shows their location. Coordinate system WGS84-UTM Zone 28 N (EPSG: 32628).

| Number	Vent	Latitude (N)	Longitude (W)
1	Montaña del Tesoro	27.832605	−17.897176
2	La Caleta	27.803759	−17.883599
3	Montaña Chamuscada	27.765188	−17.910207
4	Several vents in the La Restinga area	27.640721	−17.976894
5	Hoya del Roque	27.638071	−17.988233
6	Luna	27.656327	−18.015148
7	Montaña de la Empalizada	27.673497	−18.028299
8	Montañita Negra	27.704047	−18.134569
9	El Meridiano	27.713890	−18.158693
10	Montaña de Las Calcosas	27.723052	−18.159820
11	Montaña de Los Guirres	27.750901	−18.155244
12	Hoya del Verodal	27.758083	−18.152315
13	Montaña de Marcos	27.762598	−18.142893
14	Roque de Basco	27.766017	−18.139970
15	Arenas Blancas	27.769907	−18.125349
16	Sabinosa	27.756294	−18.101914
17	Montaña de Aguarijo	27.841026	−17.946742

Tesoro eruption are exposed in Tables 2 to 4.

4.3.1. Cone

The cone is asymmetrical, with the SE flank more developed. It shows an ellipsoidal crater with a horseshoe-shaped opening oriented to the NE in favor of the slope. The maximum axis of the cone is 830 m and that of the crater 308 m (Table 4). It is mainly formed by tephra consisting of fragments of lapilli size clasts (2–64 mm), though blocks and bombs can also be found. The ash fraction (<2 mm) is low. Cone height reaches 121 m and is conditioned by relief, being the mean value of basement slope 16°. Cone slope ranges between 0 and 66°, with a mean value of 25°. Erupted volume (V_{CE}) is 9,860,107 m^3 bulk and 2,465,027 m^3 DRE (Tables 2 and 4).

4.3.2. Lava flows

The Montaña del Tesoro eruption developed compound flows (Walker, 1972) that produced pāhoehoe lavas close to the emission center, transitioning to 'a'ā lavas (known locally as "malpaís") along with the entire littoral platform. Erratic blocks and accretion balls are common. Subaerial 'a'ā lava flows should have generated piles of submarine sheet flows (Ramalho et al., 2013) since the pahoehoe lavas would have produced hyaloclastites and pillow lavas foresets, and polygonal feeder tubes filled with hydroclasts, among other cooling structures (Perez-Torrado et al., 2015; Ramalho et al., 2013). Secondary lava breakouts are common on subaerial and submerged platforms. They are a new, morphologically distinct region of lava flow advance, formed from the core of an otherwise stopped or slowed portion of the lava flow (Magnall et al., 2018).

Considering the subaerial and submarine paths, the lava flow length reached 1715 m (Table 5 and Fig. 12). The bottom width varies from 3 to 1780 m, with a mean value of 1013 m. The thickness ranges between 1 and 38 m, with a mean value of 16 m. The length, thickness, and area occupied by lava flows depend on the terrain's morphology and the presence or absence of obstacles. Two landforms mainly conditioned these parameters, the paleo-cliff that induced spectacular lavafalls and the marine platform that was fossilized by these lavas and modeled the land surface gain of the island. The lava flows traveled 500 m through a gentle slope from the lava shield of scutulum type eruptive center, reaching 600 m in width and 5 m thick at the paleo-cliff edge (Fig. 12). They thickened and, above all, widened from the base of the cliff to the pre-eruptive coastline (CL_1). This thickening is maintained up to 1500 m from the focus, coinciding with the shelf edge, drawing a new seafront (CL_2) about 500 m from the pre-eruptive coast CL_1. The slope then steepers, and the thickness is drastically reduced. The contour lines of bathymetry suggest the occurrence of secondary lava flows or breakouts.
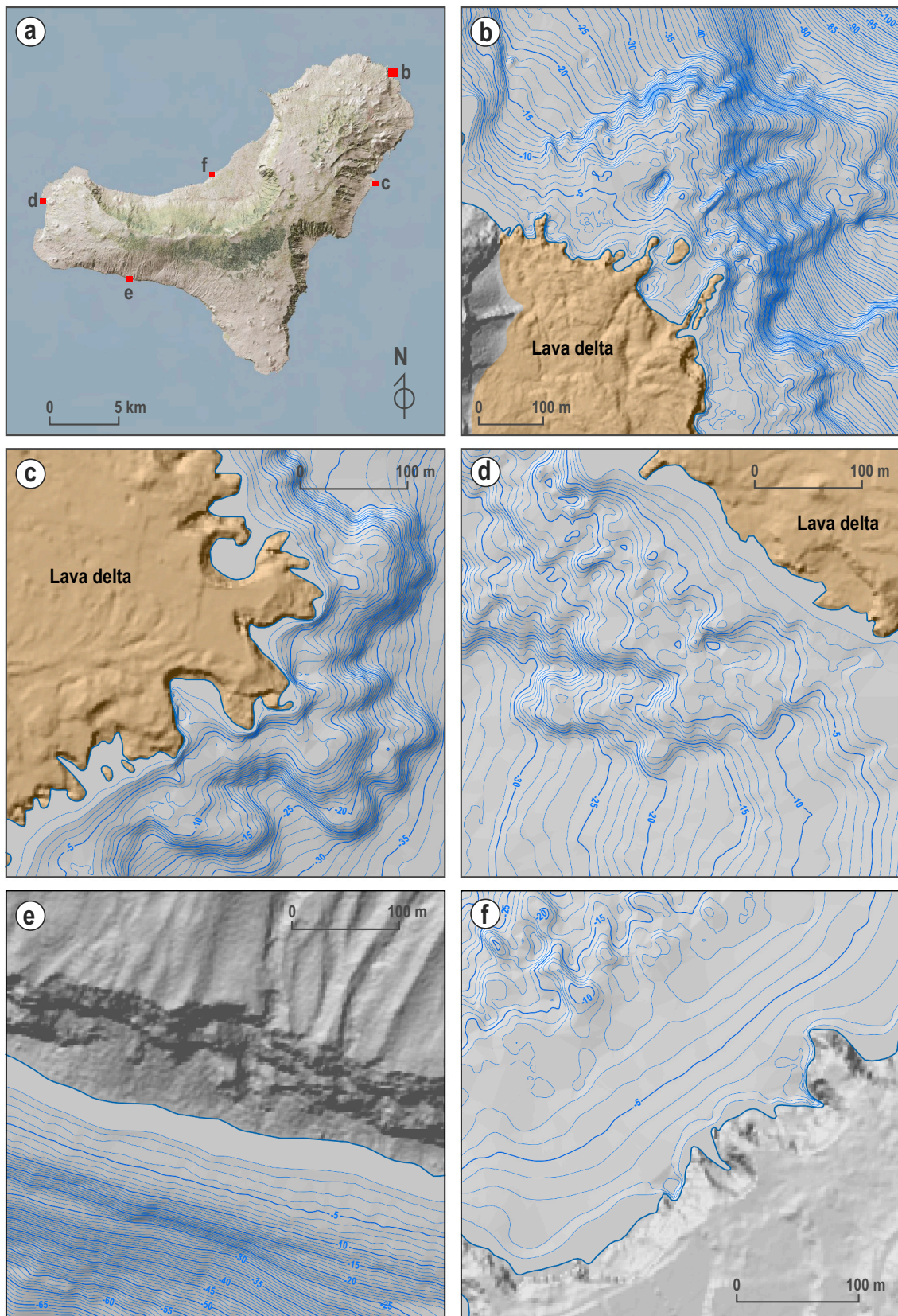
Fig. 9. Comparison of examples of shore platforms affected and unaffected by lava flows. (a) Location of examples. (b) Lava flows of Montaña del Tesoro eruption. (c) Lava flows of Montaña Chamuscada. (d) Lava flows of Hoya del Verodal. (e-f) Shore platforms are unaffected by volcanism at the Sea of Calms (Mar de las Calmas) and El Golfo.
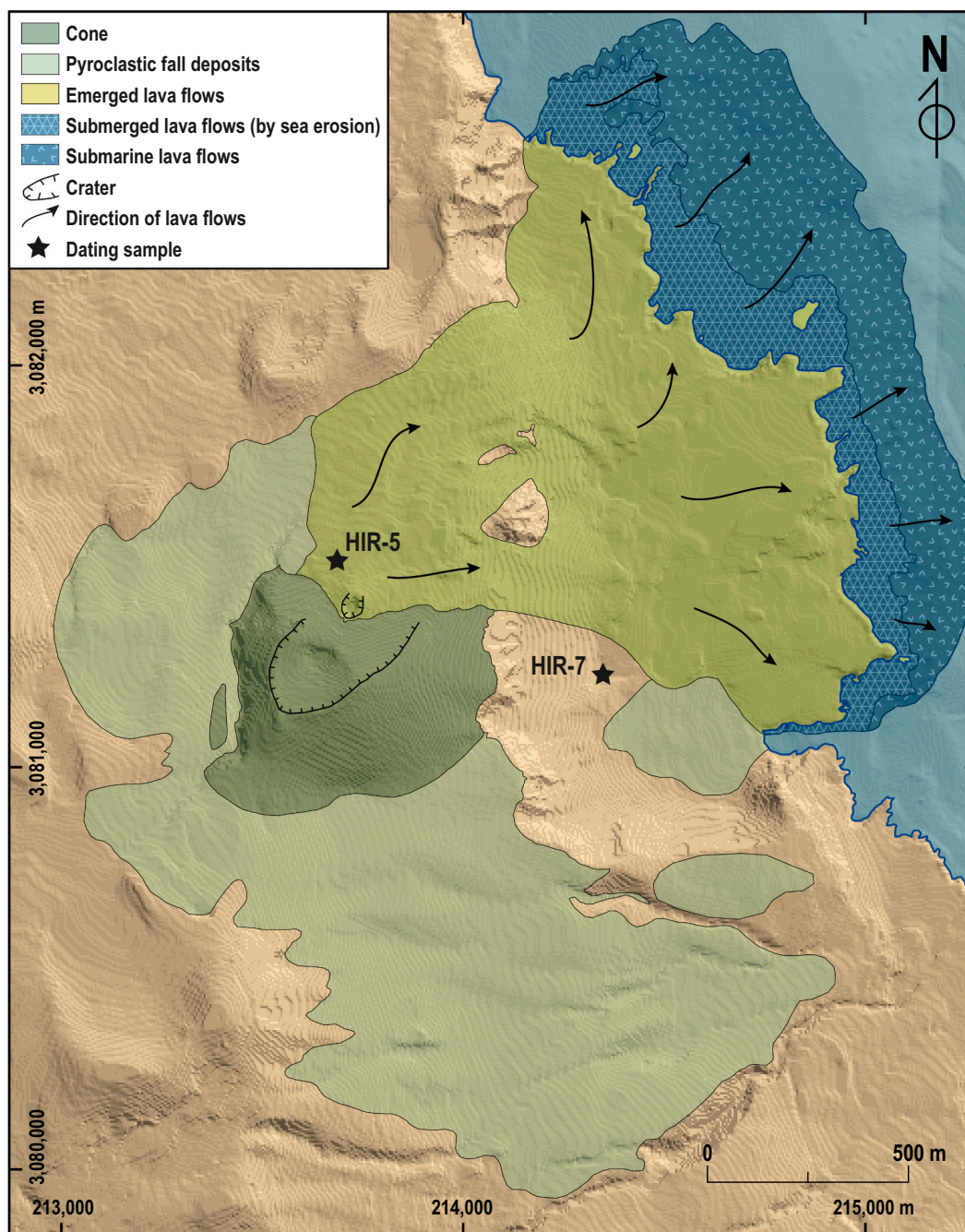
Fig. 10. Geological map of the Montaña del Tesoro eruption. Coordinate system: WGS84-UTM Zone 28 N (EPSG: 32628). DEM (reclassified to 5 m resolution) from the 1:5000 Topographic Map (Cartográfica de Canarias GRAFCAN, 2006) and 1:1000 Bathymetric Map (Dirección General de Costas, 2003).

Finally, the retreat of the post-eruption coast to the current position (CL$_3$ in Figs. 4 and 12), approximately 300 m, is considered associated only with coastal erosion processes. The erupted volume of lava flows was 29,877,373 m^3 bulk and 22,408,030 m^3 DRE, covering an area of 1,842,238 m^2 (Tables 4 and 5).

4.3.3. Pyroclastic fall deposits

Pyroclastic fall deposits extend around the cone, from 3 to 0.01 m thick, principally to the southeast due to the prevailing trade winds from N-NW. They consist mainly of lapilli, although cylindrical volcanic bombs are common in the deposits closest to the eruption vent. In the distal deposits, the predominant grain sizes are fine lapilli and ash. For practical reasons for the morphometric analysis (small volume), the scarce pyroclastic density current (PDC) deposits were included in the pyroclastic fall deposits unit. These PDC deposits are laminated, and the ash fraction dominates in their grain size distribution. The area covered by tephra fall deposits is 1,979,647 m^2. The estimated erupted volume was 2,969,471 m^3 (bulk) and 742,368 m^3 (DRE) (Table 4).

4.3.4. Erupted volume

The total bulk volume of the pyroclastic materials (12,829,578 m^3), cone and tephra fall deposits, corresponds to a volcanic eruption index (VEI) of 3 (Newhall and Self, 1982). A comparison of DRE volumes shows that this eruption was mainly effusive, erupting 87 % of its volume as lava flows, corresponding 10 % to the cinder cone and 3 % to tephra fall deposits (Table 6; Fig. 13). The total DRE volume erupted was 25,615,424 m^3.
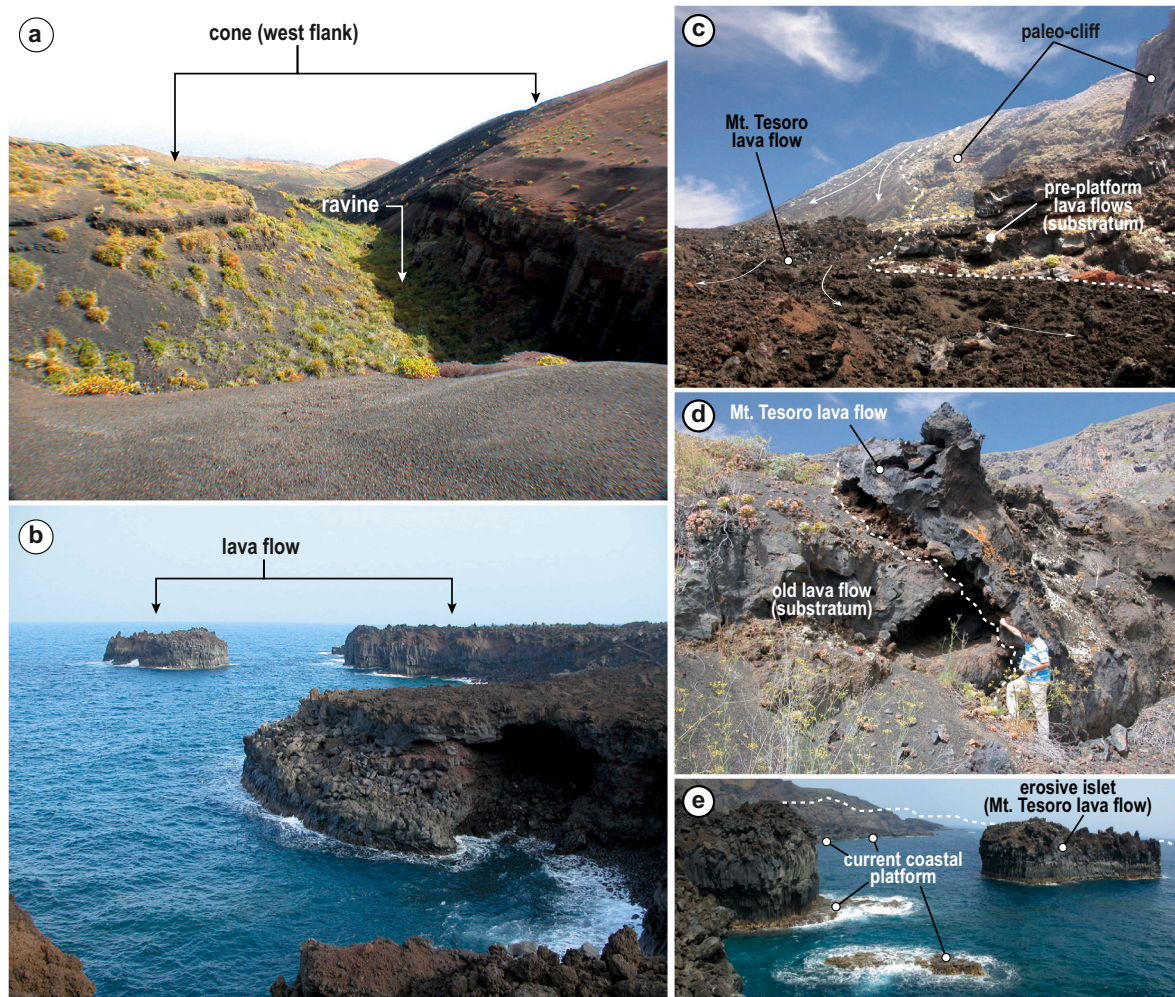
Fig. 11. (a) Erosional incision of a ravine on the main cone of Montaña del Tesoro eruption. (b) Present-day coastline and islet preserving the Montaña del Tesoro lava flow. (c) Cascade of lavas from the Montaña del Tesoro eruption. (d) Detail of the contact between the Montaña del Tesoro lava flow, forming a cascade, and the basement. (e) Low tide allows us to appreciate the current platform.

4.3.5. Landscape degradation

The total eroded bulk volume (4,106,968 m^3) comes from lava flows (73 %), pyroclastic flow deposits (14 %), and cone (13 %) (Fig. 13). The most apparent erosional degradation occurred in the lava field, mainly disturbed by marine erosion. Coastal erosion does show important signs on the old lava fronts, causing them to retreat, leaving isolated large rocks as witnesses, such as the Roque de Las Gaviotas. New cliffs were formed in the island and islets, where the lavas have a marked columnar disjunction with column heights exceeding 20 m (Fig. 11b and e). Marine erosion removed 9 % of the erupted volume of lava flows against 1 % by fluvial erosion. Besides these modifications, the most effective degradation was on the pyroclastic flow deposits, with a 20 % volume reduction. The cone is the part of the edifice best preserved, having lost a 6 % volume.

Considering the age of 1050 years BP for the Montaña del Tesoro eruption, erosion rates can be established independently for each of the volcanic units through the difference between the post-eruption and current volumes considering the elapsed time of the degradation. These data allow us to assess the differences between the volcanic units against degradation. Cone and pyroclastic fall deposits show similar erosion rates, 517 and 563 m^3/y, respectively. The total erosion rate for the lava field (2832 m^3/y) is the result of a low rate of fluvial erosion (322 m^3/y) and a higher rate of marine erosion (2510 m^3/y). This marine erosion rate also shows differences between the subaerial and submarine deposits of lava flows, 1401 and 1109 m^3/y, respectively. The rate of

coastline retreat is 0.29 m/y, considering a retreat of 300 m in 1050 years.

A fresh, young cone with a sharp profile and a pristine lava flow make up the geomorphic signature of the Montaña del Tesoro edifice, confirming that its erosional history is in the first stage of degradation (Rodriguez-Gonzalez et al., 2011). Although anthropic activity has also modified the cone and, especially, the subaerial lava delta on which the town of Tamaduste was built, the original features are mostly preserved.

5. Discussion

5.1. The rock coast of El Hierro

El Hierro exemplifies a young ocean volcanic island with no fringing reef (Woodroffe, 2014). In this early stage of evolution, its subaerial growth is governed by erosive destruction, particularly along the coast, and volcanic construction, in which the progradation of lava deltas plays a key role (Ramalho et al., 2013).

Coastal landforms on the island of El Hierro show sea-cliff profiles (Fig. 6), with practically no beaches and a narrow shore platform as a result of the significant degree of the relative effectiveness of marine versus terrestrial erosion. The geometry of these shore platforms (Fig. 6) consists of a gently sloping erosional surface extending from the base of the sea cliff to below sea level without a discernible topographic break. Marine erosion (abrasion, chemical weathering, and biological activity)

Table 4

Morphometric parameters and their derivatives of the cinder cone of the Montaña del Tesoro eruption.

Cinder cone	Symbol	Unit	Value
Crater rim maximum elevation	h	m	468
Crater rim major axis	a_{cr}	m	308
Crater rim minor axis	b_{cr}	m	212
Crater rim eccentricity	e_{cr}		0.7
Crater major axis azimuth	θ	degrees	44
Crater depth	h_{cr}	m	62
Cone major axis	a_{co}	m	830
Cone minor axis	b_{co}	m	660
Cone eccentricity	e_{co}		0.6
Cone major axis azimuth	θ	degrees	58
Cone height	H	m	121
Cone slope (beta)	α		
Median		degrees	26
Mean		degrees	25
Minimum		degrees	0
Maximum		degrees	66
Standard deviation		degrees	10
Basement slope (pre-eruption)	β		
Median		degrees	17
Mean		degrees	16
Minimum		degrees	0
Maximum		degrees	55
Standard deviation		degrees	8
Area	A	m^2	311,117
Bulk volume	V_{CE}	m^3	9,860,107

is particularly active at the base of cliffs tending to make the profile's base sharply angular. Meanwhile, terrestrial erosion produces gullying, rainwash at the ground, and slumping and other mass movements tend to make the top broadly convex upward with short-term concavities associated with local runoff or mass movements (Fig. 5b).

The coastline is considered mostly uniform in lithology and structure (stacks of lava flows), but wave energy varies from highly exposed sectors in the western and northern extremes of the island to the sheltered coasts on the southern (*Mar de las Calmas*), central-northern, and eastern sides of the island. As wave energy increases, so does the width of the affected area (Fig. 6). Thus, the shelf width is directly related to wave exposure, as observed in other volcanic ocean islands as, for example, Faial Island (Quartau et al., 2010; Zhao et al., 2019) and Terceira Island (Quartau et al., 2014) in the Azores archipelago, and La Gomera in the Canaries (Llanes et al., 2009). However, this general setting shows local exceptions, with some >25 m wide shore platforms occurring in the areas where the wave attack is more attenuated. These discrepancies are related to a geology that is different from the overall stacks of lava flows, for example, due to the presence of cinder cones or areas affected by giant landslide scars (e.g., Las Playas landslide, profile 8 in Fig. 6). Another possibility is that the contemporary shore platform could have developed on a previous platform, which might explain the anomalous location reflected in profile 3 in Fig. 6, situated in the center of the El Golfo giant landslide.

Although contemporary shore platform and sea cliff morphology result mainly from the wave regime and rock resistance, it also reflects how the relative sea level (RSL) attained its present stillstand during the last thousand years (Trenhaile, 2010). The Holocene RSL rise is imprecisely defined in the Canary Islands. However, models agree to consider two evolutive stages. The sea level rose rapidly (10–15 mm/y) from the Last Glacial Maximum (LGM), about 20,000 years ago (Lambeck et al., 2014; Osman et al., 2021), to about 7 ka BP, remaining practically stable afterward, forming shore platforms (Buchner et al., 2015; Maréchal et al., 2020; Meco et al., 2018; Melo et al., 2022; Rijsdijk et al., 2013). This model is typical for western African coasts (Cooper et al., 2018; Lambeck et al., 2014; Trenhaile, 2010).

On the other hand, the uplift associated with volcanic events could modify shore platforms' apparent steady vertical position. For example, the magma that intruded beneath El Hierro from 2011 to 2014

Table 5

Morphometric parameters and their derivatives of the lava flows of the Montaña del Tesoro eruption.

Lava flows	Symbol	Unit	Value
Length	L	m	1715
Bottom width	w_b		
Median		m	1021
Mean		m	1013
Minimum		m	3
Maximum		m	1780
Standard deviation		m	600
Height (thickness)	h		
Median		m	15
Mean		m	16
Minimum		m	1
Maximum		m	38
Standard deviation		m	12
Basement slope	β		
Median		degrees	13
Mean		degrees	17
Minimum		degrees	0
Maximum		degrees	45
Standard deviation		degrees	12
Area	A_{LE}	m^2	1,842,238
Subaerial current surface before pre-eruption coastline CL_1 (Sector 1)	A_{L1}	m^2	660,771
Subaerial post-eruption surface before pre-eruption coastline CL_1 (Sector 1)	A_{L1E}	m^2	662,871
Subaerial current surface between pre-eruption (CL_1) and current (CL_3) coastlines (Sector 2)	A_{L2}	m^2	473,964
Subaerial post-eruption surface between pre-eruption (CL_1) and current (CL_3) coastlines (Sector 2)	A_{L2E}	m^2	473,964
Subaerial current surface between post-eruption (CL_1) and current (CL_3) coastlines (Sector 3)	A_{L3}	m^2	4195
Subaerial post-eruption surface between post-eruption (CL_1) and current (CL_3) coastlines (Sector 3)	A_{L3E}	m^2	275,091
Submerged current surface (Sector 4)	A_{L4}	m^2	430,312
Submerged post-eruption surface (Sector 4)	A_{L4E}	m^2	430,312
Bulk volume	V_{LE}	m^3	29,877,373
Subaerial current volume before pre-eruption coastal line CL_1 (Sector 1)	V_{L1}	m^3	8,618,374
Subaerial post-eruption volume before pre-eruption coastal line CL_1 (Sector 1)	V_{L1E}	m^3	8,640,753
Subaerial current volume between pre-eruption (CL_1) and current (CL_3) coastlines (Sector 2)	V_{L2}	m^3	10,376,888
Submerged current volume between pre-eruption (CL_1) and current (CL_3) coastlines (Sector 2)	V_{L2s}	m^3	2,765,137
Subaerial post-eruption volume between pre-eruption (CL_1) and current (CL_3) coastlines (Sector 2)	V_{L2E}	m^3	10,692,941
Submerged post-eruption volume between pre-eruption ($CL1$) and current ($CL3$) coastlines (Sector 2)	V_{L2sE}	m^3	2,765,137
Subaerial current volume between current (CL_3) and post-eruption (CL_2) coastlines (Sector 3)	V_{L3}	m^3	24,366
Submerged current volume between current (CL_3) and post-eruption (CL_2) coastlines (Sector 3)	V_{L3s}	m^3	2,437,023
Subaerial post-eruption volume between current (CL_3) and post-eruption (CL_2) coastlines (Sector 3)	V_{L3E}	m^3	1,495,223
Submerged post-eruption volume between current (CL_3) and post-eruption (CL_2) coastlines (Sector 3)	V_{L3sE}	m^3	3,601,068
Submerged current volume between post-eruption coastline CL_2 and lava front (Sector 4)	V_{L4s}	m^3	2,682,251
Submerged post-eruption volume between post-eruption coastline CL_2 and lava front (Sector 4)	V_{L4sE}	m^3	2,682,251
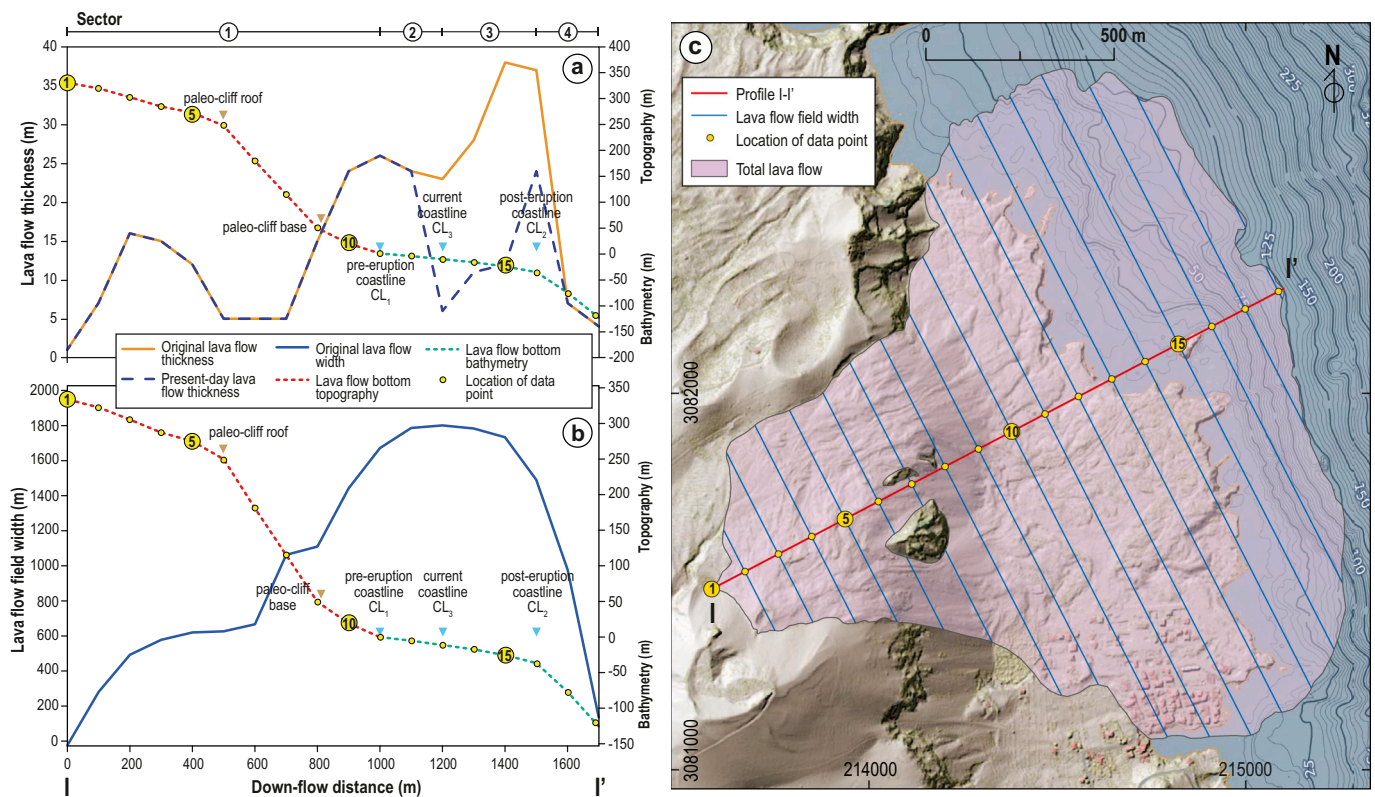
Fig. 12. Thickness (a) and width (b) variations of the lava flows of Montaña del Tesoro eruption (solid line) determined from cross-sections perpendicular to flow direction; data obtained every 100 m (c), following the topography and bathymetry of the traveled path (dotted line). The lava flow field was sectorized to facilitate the study: Sector 1 includes from the vent to the pre-eruption coastline (CL$_1$); Sector 2 from the pre-eruption coastline (CL$_1$) to the current coastline (CL$_3$); Sector 3 from the current coastline (CL$_3$) to post-eruption-coastline (CL$_2$); and Sector 4 from the post-eruption coastline (CL$_2$) to the lava flow front.

Table 6
Bulk and dense rock equivalent (DRE) volumes of Montaña del Tesoro eruption.

Unit	Bulk volume (m^3)	Bulk volume (%)	DRE Volume (m^3)	DRE volume (%)
Cone	9,860,107	23	2,465,027	10
Lava flows	29,877,373	70	22,408,030	87
Tephra fall deposits	2,969,471	7	742,368	3
Total	42,706,951	100	25,615,424	100

(comprising the Tagoro submarine eruption and six post-eruptive intrusions) produced >10 cm of horizontal ground deformation in the island and > 20 cm of uplift in the central and western part, as revealed by GNSS and InSAR data sets (Benito-Saz et al., 2017, 2019). Although the uplifts related to magmatic and seismic processes are common, their influence on the evolution of shore platforms has received little attention. Their study has been practically confined to New Zealand (Kennedy and Beban, 2005). Although the order of magnitude of magmatic uplifts is usually lower than those of seismic origin, decimetric against metric scale, they must also influence the coastline's erosional processes, contributing to developing a highly dynamic youthful shore platform environment (Kennedy and Beban, 2005).

In this setting, a lava flow forms a delta on the contemporary shore platform, reaching the coastline (Fig. 9). The lava delta's subaerial part is locally named "*islas bajas*" or "*fajãs lávicas*" in the Portuguese-speaking Archipelagos. This feature is of great interest for the relative dating of such volcanic eruptions and allows refining the previous categorization of recent eruptions based on lavas forming cliffs (>20 ka) and lavas forming coastal platforms (<20 ka) (Carracedo et al., 2001). Thus, the lava deltas on the contemporary shore platform indicate ages contemporary with the present highstand, i.e., <7 ka BP eruptions. According to this geomorphological criterion, at least 21 eruptions deposited lavas on the contemporary shore platforms around El Hierro in the last 7000 years, e.g., the Montaña del Tesoro eruption.

5.2. The volcanism

The Montaña del Tesoro eruption is typical of monogenetic basaltic volcanism (Németh, 2010; Walker, 2000), and morphometric values are characteristic of Strombolian-type eruptions from fissure vents (e.g., Dóniz-Páez, 2015; Haag et al., 2019; Kereszt005uri et al., 2012, 2013; Rodriguez-Gonzalez et al., 2012a, 2012b). Its DRE volume (25,615,424 m^3) is high in the Canaries setting. For example, it is in the upper part of the range (103,006 to 30,441,232 m^3) observed for the 24 Holocene eruptions of Gran Canaria (Rodriguez-Gonzalez et al., 2012a).

Considering the cone morphology of Montaña del Tesoro and the pyroclastic materials that form it, it can be assimilated to a type 3 in the classification of Martin and Németh (2006), originated by Strombolian to sub-Plinian eruptive mechanisms. The morphometric results of the cone are comparable to those measured on the Holocene volcanic edifices of Gran Canaria island (Rodriguez-Gonzalez et al., 2012a), values also expected for Strombolian eruptions.

The larger length of the main axis and shorter cone height relative to an ideal cone are due to the edifice developed over irregular topography. Though this feature could affect the ellipticity of the crater, its location is mainly related to the weakest area of the cone, which is typically situated over the magma feeding fissure. Orography, together with the structural features of feeder dyke, also influences crater depth (Tibaldi, 1995).

As a single eruptive event, variability in lava rheology is minimal, and differences in local flow behavior are related to changes in effusion,
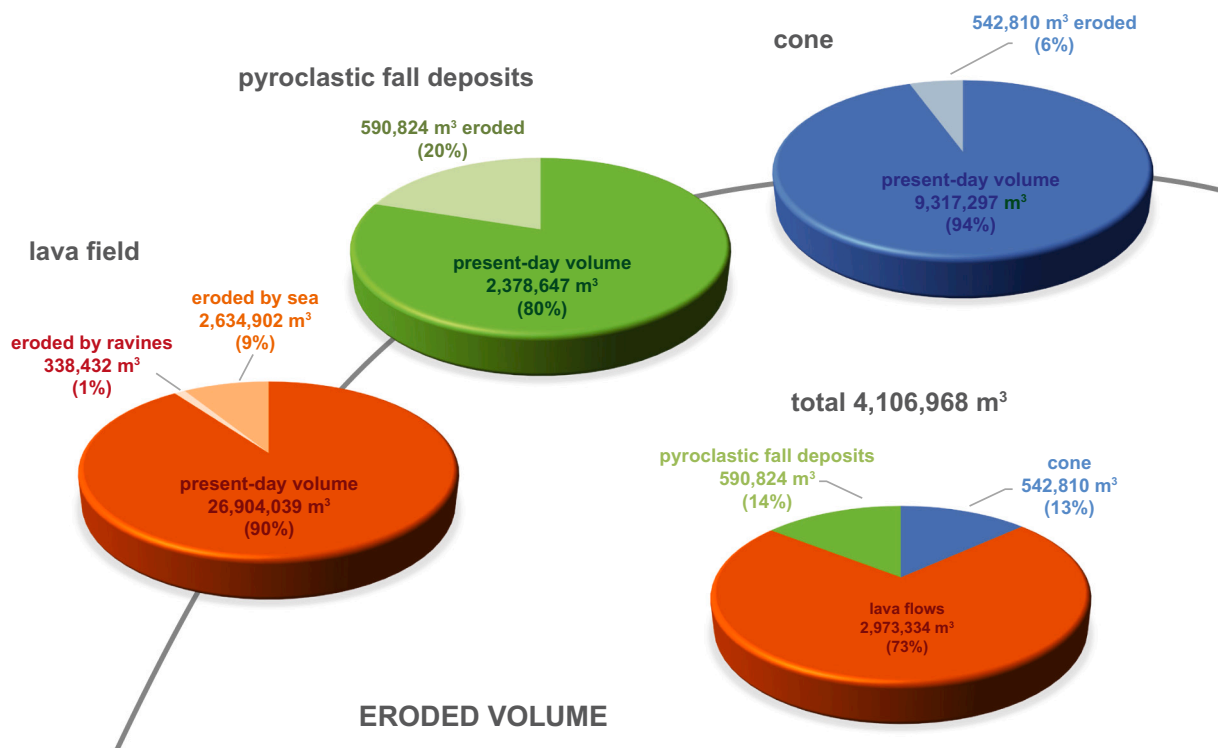
Fig. 13. Bulk eroded volumes from the volcanic units of the Montaña del Tesoro eruption concerning their present-day volumes and the total eroded volume.

local flux rate influenced by topography, and the subaerial or submarine environment (e.g., Pinkerton and Wilson, 1994). The studied lava flows are comparable to those observed in the Canary Islands Archipelago (Hernández Pacheco, 1987; Longpré and Felpeto, 2021; Prieto-Torrell et al., 2021; Romero Ruiz, 1990).

The 29,877,373 m^3 bulk volume of lava flows is high in the Canary Islands. For example, it exceeds that observed in the Holocene eruptions of Gran Canaria, where lava flow volumes range from 900 to 10,738,722 m^3 (Rodriguez-Gonzalez et al., 2012a). Nevertheless, relative to La Palma's historical eruptions, considering that la Palma is in the same juvenile stage as El Hierro, this total bulk volume of lava is usual, although low compared with the recent 2021 eruption at La Palma, where lava flow volume exceeded 120,000,000 m^3. This relatively high lava volume (87 % DRE volume) easily breaks the cone and, as a result, erratic blocks of cone material can be observed on the surface of the lava flows up to thousands of meters from the eruption vent.

Such other Canary lava flows, the Montaña del Tesoro lava length (1715 m) is shorter than extreme lengths measured in lava flows from other volcanic oceanic islands, e.g., 51 km for an eruption of the Mauna Loa volcano in Hawai'i (Lockwood and Lipman, 1987), or 140 km for the Thjórsá's eruption in Iceland (Hjartarson, 1988). It is also shorter than comparable eruptions, e.g., Gran Canaria (median 2.6 km for 21 Holocene eruptions; Rodriguez-Gonzalez et al., 2012a, 2012b) and Hawai'i (median 9.0 km for 87 individual flows during 33 historical eruptions; Malin, 1980). The coastline's distance and, mostly, the pre-existing shore platform conditioned the shortness of the studied lava flows, favoring breakouts and the lava field widening.

The dispersion area of pyroclastic fall deposits is asymmetrical and elongated to SE. This elongation responds to the eruptive column height and the prevailing N–NW wind (trade winds). The influence of predominant trade winds of the subtropical Azores anticyclone during Holocene on the pyroclastic fall dispersion in the north side of the Canary Islands is well reported (Rodriguez-Gonzalez et al., 2012a, 2018). Besides this extent (1,979,647 m^2), their relatively low bulk volume (7 %) and thickness only slightly modified the pre-existing surface, introducing topography-mantling changes (Manville et al., 2009). Such

deposits have a low preservation potential, becoming remobilized by wind and water, especially in the most distal areas from the emission center.

5.3. Landscape evolution

The geomorphological evolution of the volcanic ocean island's coastline results from volcanic aggradation processes and erosive degradation (Ramalho et al., 2013; Rodriguez-Gonzalez et al., 2011). The coasts affected by Holocene volcanic activity in El Hierro Island provide an opportunity to observe the geomorphological effects of erosion at timescales reaching several millennia. El Hierro and La Palma islands are in the juvenile stage of evolution, with high eruption rates and fast volcanic growth (Carracedo et al., 2001). This context limits the progradation of lava deltas. The coastal shelf of these juvenile islands is usually between 300 and 500 m wide, which is the maximum distance lava deltas will reach because gravitational forces make lava flows unstable on the steeper slopes beyond the shelf edge (Ramalho et al., 2013). In contrast, in stages of quiescence or rejuvenation of a volcanic ocean island, the lava deltas reach considerably greater distances, as happened with the Pliocene lava delta of Roque Nublo in Gran Canaria Island (Perez-Torrado et al., 2015).

Fig. 14 shows the shoreline evolution at pre-, post-eruption, and present-day stages. At the pre-eruption stage (1050 years ago), the landscape of the study area was characterized by an active cliff and a narrow, sloping shore platform (Fig. 14a). In the case of an eruption on the coastal cliff, this scenario is conducive to the progradation of lava deltas. This is the case of the Montaña del Tesoro volcano (Fig. 14b) and others from ocean island volcanoes and other coastal volcanoes (Bosman et al., 2014; Lipman and Moore, 1996; Prieto-Torrell et al., 2021). Landform degradation by terrestrial processes, including fluvial processes, is very low, affecting mainly the northwestern flank of the main cone (Fig. 11a). Marine erosion shows important signs on the advancing fronts of the lavas, causing them to retreat several hundreds of meters and leaving large isolated cliffed lavas as witnesses (Fig. 11b and e). The results are active sea cliffs (Emery and Kuhn, 1982), resistant at the top
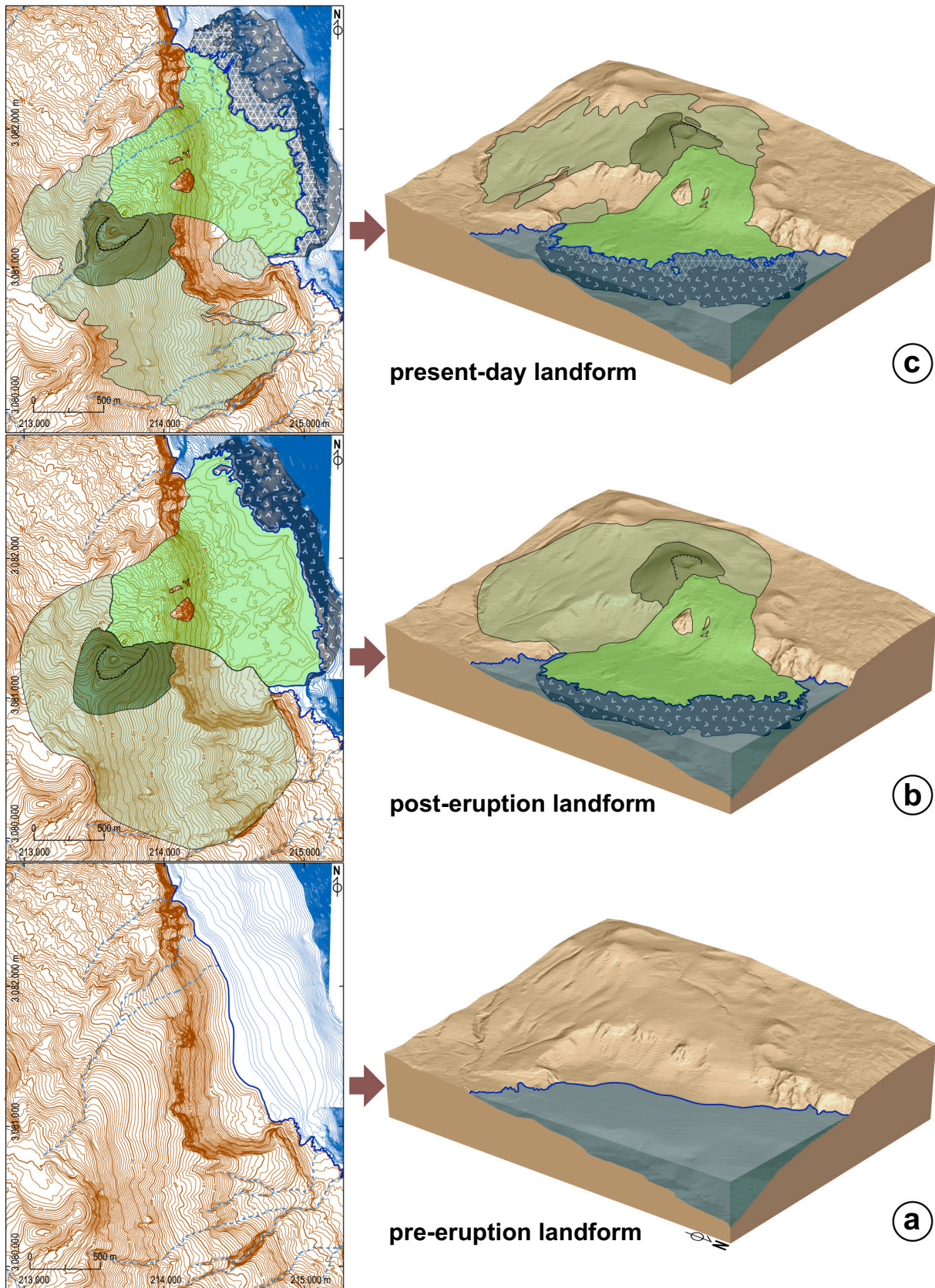
Fig. 14. Shoreline evolution of El Hierro Island's littoral affected by the Montaña del Tesoro eruption. Shoreline configuration at a generic time-frame in the present sea-level highstand (a) where the Montaña del Tesoro eruption occurs (dated at 1050 years BP) (b). A more efficient marine than fluvial erosion leads to the current scenario (c). Same legend as Fig. 10.

and with a sharp angle at the sea cliff base, in the main coastline and the islets. In this setting, the remains of the subaerial and submerged lava flows are quickly mobilized by waves, leaving a rugged, poorly sorted deposit (Mitchell et al., 2008). The low quantity of this volcaniclastic debris would imply the movement of relatively coarse material to the island's submarine slope during storms.

The estimated coastline retreat rate (0.29 m/y) is in the lower part of the range (0.08–12.5 m/y) of compiled data on deltas formed during historical and Holocene eruptions (age ≤ 6 ka) from both 'a'ā and pāhoehoe lava flows, and from diverse localities (the Azores and Hawaiian islands and Ascension Island) (Zhao et al., 2020). This is because the wave regime in the Canary Islands (even on the windward side) is less energetic than on those islands. This erosion rate categorizes the northeastern coast of El Hierro as a medium resistance rock coast (Prémaillon et al., 2018).

In summary, the availability of seamless topography-bathymetry data sets contributes to the broader knowledge of coastal evolution at oceanic volcanic islands and reduces the need for expensive specific bathymetric campaigns. This work can teach some lessons at the scale of an oceanic volcanic island and an eruptive event. The combination of topography and bathymetry shows a complete picture of the effects of those eruptions forming lava deltas. The modification of bathymetry helps to identify and accurately reconstruct recent eruptions. This work provides methods and results of great interest with different implications, among which we can mention coastal planning (e.g., rock coast evolution) and volcanic risk assessment (e.g., the importance of Holocene sea-level rise on the development of shore platforms facilitating the progradation of lava deltas).

6. Conclusions

El Hierro Island presents a rocky coast with an active sea-cliff profile, reflecting the early evolutionary stage of a young ocean volcanic island with no fringing reef. The marine erosion during the Holocene sea-level highstand (<7 ka) has developed a shore platform, mainly conditioned by the energy of the waves. This geomorphological feature allows us to date relatively those eruptions that reached the coast and formed lava deltas affecting this contemporary insular shelf. According to this criterion, at least 17 eruptions occurred in El Hierro during the last 7000 years. One of these eruptions was the Montaña del Tesoro, a case study for morphometric modeling integrating subaerial and submarine data at a scale of a volcanic edifice.

The coastal landscape change after the eruption of Montaña del Tesoro reconciles data on land and offshore consistently. Their lava flows spilled over a paleo-cliff edge, forming cascades, and they continued over the shore platform, facilitating the progradation of a lava delta. We perform the morphometric analysis of cone, pyroclastic fall deposits, and lava field for the post-eruption and present-day stages. Methodologically, as a novelty, we introduced a discretization of lava flow field according to the coastline evolution and lava front sectors, and their subaerial or submarine placement. This strategy was used for the morphometric analysis of the post-eruption and present-day stages.

A VEI 3 was estimated for the eruption. The total bulk volume was 42,706,951 m³, and the DRE volume was 25,615,424 m³. It was mainly effusive, erupting 87 % of DRE volume as lava flows, 10 % formed the cinder cone, and 3 % the tephra fall deposits. The degradation mainly affected the lava field, where marine erosion removed 9 % of the erupted volume of lava flows against 1 % by fluvial erosion. The slow coastline retreat rate estimated (0.29 m/y) is interpreted as related to the considerable lava cliff resistance to erosion and the less energetic wave regime of the Canary Islands.

The El Hierro Island and the Montaña del Tesoro volcano case study provide a further analogue for volcanism affecting ocean islands' coastline of interest for coastal planning (e.g., rock coast degradation) and volcanic risk assessment (e.g., the importance of Holocene sea-level rise on the development of shore platforms facilitating the progradation

of lava deltas).

Declaration of competing interest

The authors declare that they have no known competing financial interests or personal relationships that could have influenced the work reported in this paper.

Data availability

The source of all data used are specified in the article.

References

Acosta, J., Uchupi, E., Smith, D., Muñoz, A., Herranz, P., Palomo, C., Llanes, P., Ballesteros, M., 2005. Comparison of volcanic rifts on La Palma and El Hierro, Canary Islands and the Island of Hawaii. In: Clift, P., Acosta, Juan (Eds.), Geophysics of the Canary Islands: Results of Spain's Exclusive Economic Zone Program. Springer, Netherlands, Dordrecht, pp. 59–90. https://doi.org/10.1007/1-4020-4352-X_3.

AEMET, 2012. In: <collab>Ministerio de Agricultura, Alimentación y Medio Ambiente</collab> (Ed.), Climate Atlas of the Archipelagos of the Canary Islands, Madeira And the Azores, Air Temperature And Precipitation (1971-2000).

Ancochea, E., Huertas, M.J., Hernán, F., Brändle, J.L., 2010. Volcanic evolution of São Vicente, Cape Verde Islands: the Praia Grande landslide. J. Volcanol. Geotherm. Res. 198, 143–157. https://doi.org/10.1016/j.jvolgeores.2010.08.016.

Ancochea, E., Hernán, F., Huertas, M.J., Brändle, J.L., 2012. A basic radial dike swarm of Boa Vista (Cape Verde Archipelago); its significance in the evolution of the island. J. Volcanol. Geotherm. Res. 243–244, 24–37. https://doi.org/10.1016/j.jvolgeores.2012.06.029.

Becerril, L., Cappello, A., Galindo, I., Neri, M., Del Negro, C., 2013. Spatial probability distribution of future volcanic eruptions at El Hierro Island (Canary Islands, Spain). J. Volcanol. Geotherm. Res. 257, 21–30. https://doi.org/10.1016/j.jvolgeores.2013.03.005.

Becerril, L., Bartolini, S., Sobradelo, R., Martí, J., Morales, J.M., Galindo, I., 2014. Long-term volcanic hazard assessment on El Hierro (Canary Islands). Nat. Hazards Earth Syst. Sci. 14, 1853–1870. https://doi.org/10.5194/nhess-14-1853-2014.

Becerril, L., Galve, J.P., Morales, J.M., Romero, C., Sánchez, N., Martí, J., Galindo, I., 2016. Volcano-structure of El Hierro (Canary Islands). J.Maps 12, 43–52. https://doi.org/10.1080/17445647.2016.1157767.

Benito-Saz, M.A., Parks, M.M., Sigmundsson, F., Hooper, A., García-Cañada, L., 2017. Repeated magmatic intrusions at El Hierro Island following the 2011–2012 submarine eruption. J. Volcanol. Geotherm. Res. 344, 79–91. https://doi.org/10.1016/j.jvolgeores.2017.01.020.

Benito-Saz, M.A., Sigmundsson, F., Charco, M., Hooper, A., Parks, M., 2019. Magma flow rates and temporal evolution of the 2012–2014 post-eruptive intrusions at El Hierro, Canary Islands. J.Geophys.Res.Solid Earth 124, 12576–12592. https://doi.org/10.1029/2019JB018219.

Bird, E.C.F., 2008. Coastal Geomorphology: An Introduction, 2nd ed. Wiley.

Bosman, A., Casalbore, D., Romagnoli, C., Chiocci, F.L., 2014. Formation of an 'a'ā lava delta: insights from time-lapse multibeam bathymetry and direct observations during the Stromboli 2007 eruption. Bull. Volcanol. 76, 838. https://doi.org/10.1007/s00445-014-0838-2.

Buchner, E., Kröchert, J., Schmieder, M., 2015. An updated and refined Holocene uplift history of southern Tenerife (Canary Islands) and the possible consequences for future volcanic activity. Geol. Mag. 152, 1137–1144. https://doi.org/10.1017/S0016756815000308.

Carracedo, J.C., 1994. The Canary Islands: an example of structural control on the growth of large oceanic-island volcanoes. J. Volcanol. Geotherm. Res. 60, 225–241. https://doi.org/10.1016/0377-0273(94)90053-1.

Carracedo, J.C., 1996. A simple model for the genesis of large gravitational landslide hazards in the Canary Islands. Geol. Soc. Lond., Spec. Publ. 110, 125. https://doi.org/10.1144/GSL.SP.1996.110.01.10.

Carracedo, J.C., 1999. Growth, structure, instability and collapse of Canarian volcanoes and comparisons with Hawaiian volcanoes. J. Volcanol. Geotherm. Res. 94, 1–19. https://doi.org/10.1016/S0377-0273(99)00095-5.

Carracedo, J.C., Day, S., Guillou, H., Rodriguez Badiola, E., Canas, J.A., Perez Torrado, F. J., 1998. Hotspot volcanism close to a passive continental margin: the Canary Islands. Geol. Mag. 135, 591–604. https://doi.org/10.1017/S0016756898001447.

Carracedo, J.C., Badiola, E.R., Guillou, H., de la Nuez, J., Pérez Torrado, F.J., 2001. Geology and volcanology of La Palma and El Hierro, Western Canaries. Estud. Geol. 57, 175–273. https://doi.org/10.3989/egeol.01575-6134.

Cartográfica de Canarias GRAFCAN, 2006. Base Topográfica a escala 1:5.000 de El Hierro (2004-2006).

Cartográfica de Canarias GRAFCAN, 2021. GeoServer.

Chiri, H., Pacheco, M., Rodríguez, G., 2013. Spatial variability of wave energy resources around the Canary Islands. WIT Trans. Ecol. Environ. 169, 15–26. https://doi.org/10.2495/CP130021.

Cooper, J.A.G., Green, A.N., Compton, J.S., 2018. Sea-level change in southern Africa since the Last Glacial Maximum. Quat. Sci. Rev. 201, 303–318. https://doi.org/10.1016/j.quascirev.2018.10.013.

Davies, J.L., 1980. Geographical Variation to Coastal Development, 2nd ed. Longman.

Di Paola, G., Rodríguez, G., Rosskopf, C.M., 2020. Short- to mid-term shoreline changes along the southeastern coast of Gran Canaria Island (Spain). Rend.Lincei Sci.Fis.Nat. 31, 89–102. https://doi.org/10.1007/s12210-020-00872-3.

Di Traglia, F., Nolesini, T., Solari, L., Ciampalini, A., Frodella, W., Steri, D., Allotta, B., Rindi, A., Marini, L., Monni, N., Galardi, E., Casagli, N., 2018. Lava delta deformation as a proxy for submarine slope instability. Earth Planet. Sci. Lett. 488, 46–58. https://doi.org/10.1016/j.epsl.2018.01.038.

Di Traglia, F., Fornaciai, A., Casalbore, D., Favalli, M., Manzella, I., Romagnoli, C., Chiocci, F.L., Cole, P., Nolesini, T., Casagli, N., 2022. Subaerial-submarine morphological changes at Stromboli volcano (Italy) induced by the 2019–2020 eruptive activity. Geomorphology 400, 108093. https://doi.org/10.1016/j.geomorph.2021.108093.

Dirección General de Costas, 2003. Estudio ecocartográfico del litoral de las islas de El Hierro y La Gomera (Tenerife).

Dóniz-Páez, J., 2015. Volcanic geomorphological classification of the cinder cones of Tenerife (Canary Islands, Spain). Geomorphology 228, 432–447. https://doi.org/10.1016/j.geomorph.2014.10.004.

Emery, K.O., Kuhn, G.G., 1982. Sea cliffs: their processes, profiles, and classification. GSA Bull. 93, 644–654. https://doi.org/10.1130/0016-7606(1982)93<644:SCTPPA>2.0.CO;2.

Gee, M.J.R., Masson, D.G., Watts, A.B., Mitchell, N.C., 2001a. Offshore continuation of volcanic rift zones, El Hierro, Canary Islands. J. Volcanol. Geotherm. Res. 105, 107–119. https://doi.org/10.1016/S0377-0273(00)00241-9.

Gee, Martin J.R., Watts, A.B., Masson, D.G., Mitchell, N.C., 2001b. Landslides and the evolution of El Hierro in the Canary Islands. Mar. Geol. 177, 271–293. https://doi.org/10.1016/S0025-3227(01)00153-0.

Geldmacher, J., Hoernle, K., Bogaard, P.v.d., Duggen, S., Werner, R., 2005. New 40Ar/39Ar age and geochemical data from seamounts in the Canary and Madeira volcanic provinces: support for the mantle plume hypothesis. EarthPlanet.Sci.Lett. 237, 85–101. https://doi.org/10.1016/j.epsl.2005.04.037.

Glass, J.B., Fornari, D.J., Hall, H.F., Cougan, A.A., Berkenbosch, H.A., Holmes, M.L., White, S.M., De La Torre, G., 2007. Submarine volcanic morphology of the western Galápagos based on EM300 bathymetry and MR1 side-scan sonar. Geochem. Geophys. Geosyst. 8 https://doi.org/10.1029/2006GC001464.

Goda, Y., 2010. Random Seas And Design of Maritime Structures. In: Advanced Series on Ocean Engineering. World Scientific. https://doi.org/10.1142/7425.

Gómez, M., Pérez-Gómez, B., De Alfonso, M., Pérez, S., Ruiz, M.I., 2015. Waves and tides in the Canary Current Large Marine Ecosystem. In: Oceanographic And Biological Features in the Canary Current Large Marine Ecosystem. IOC Technical Serie. IOC-UNESCO, Paris, pp. 115–131.

Gómez-Pazo, A., Pérez-Alberti, A., Trenhaile, A., 2021. High resolution mapping and analysis of shore platform morphology in Galicia, northwestern Spain. Mar. Geol. 436, 106471 https://doi.org/10.1016/j.margeo.2021.106471.

Guerra-Medina, D., Rodríguez, G., 2021. Spatiotemporal variability of extreme wave storms in a beach tourism destination area. Geosciences 11, 1–18. https://doi.org/10.3390/geosciences11060237.

Guillou, H., Carracedo, J.C., Torrado, F.P., Badiola, E.R., 1996. K-Ar ages and magnetic stratigraphy of a hotspot-induced, fast grown oceanic island: El Hierro, Canary Islands. J. Volcanol. Geotherm. Res. 73, 141–155. https://doi.org/10.1016/0377-0273(96)00021-2.

Guillou, H., Torrado, F.J.P., Hansen Machin, A.R., Carracedo, J.C., Gimeno, D., 2004. The Plio-Quaternary volcanic evolution of Gran Canaria based on new K-Ar ages and magnetostratigraphy. J. Volcanol. Geotherm. Res. 135, 221–246. https://doi.org/10.1016/j.jvolgeores.2004.03.003.

Haag, M.B., Baez, W.A., Sommer, C.A., Arnosio, J.M., Filipovich, R.E., 2019. Geomorphology and spatial distribution of monogenetic volcanoes in the southern Puna Plateau (NW Argentina). Geomorphology 342, 196–209. https://doi.org/10.1016/j.geomorph.2019.06.008.

Hjartarson, A., 1988. The Thjorsa lava-the largest Holocene lava flow on Earth. Natturufroeingurinn 58, 1–16.

Hoernle, K., Hauff, F., van den Bogaard, P., 2004. 70 m.y. history (139–69 Ma) for the Caribbean large igneous province. Geology 32, 697–700. https://doi.org/10.1130/G20574.1.

Holik, J.S., Rabinowitz, P.D., Austin Jr., J.A., 1991. Effects of Canary hotspot volcanism on structure of oceanic crust off Morocco. J.Geophys.Res.Solid Earth 96, 12039–12067. https://doi.org/10.1029/91JB00709.

Iglesias, G., Carballo, R., 2011. Wave resource in El Hierro—an island towards energy self-sufficiency. Renew. Energy 36, 689–698. https://doi.org/10.1016/j.renene.2010.08.021.

Instituto Geográfico Nacional, 2015. Centro de Descargas: Modelo Digital del Terreno - MDT02.

ISTAC, 2021. Estadística del Territorio. Instituto Canario de Estadística.

Jeffery, A.J., Gertisser, R., 2018. Peralkaline felsic magmatism of the Atlantic islands. Front. Earth Sci. 6 https://doi.org/10.3389/feart.2018.00145.

Kennedy, D.M., 2015. Where is the seaward edge? A review and definition of shore platform morphology. Earth Sci. Rev. 147, 99–108. https://doi.org/10.1016/j.earscirev.2015.05.007.

Kennedy, D.M., Beban, J.G., 2005. Shore platform morphology on a rapidly uplifting coast, Wellington, New Zealand. Earth Surf. Process. Landf. 30, 823–832. https://doi.org/10.1002/esp.1192.

Kennedy, D.M., Stephenson, W.J., Naylor, L.A., 2014. Chapter 1 introduction to the rock coasts of the world. In: Geological Society, London, Memoirs, 40, p. 1. https://doi.org/10.1144/M40.1.

Keresztur, G., Jordan, G., Németh, K., Dóniz-Páez, J.F., 2012. Syn-eruptive morphometric variability of monogenetic scoria cones. Bull. Volcanol. 74, 2171–2185. https://doi.org/10.1007/s00445-012-0658-1.

Keresztur, G., Geyer, A., Martí, J., Németh, K., Dóniz-Páez, F.J., 2013. Evaluation of morphometry-based dating of monogenetic volcanoes—a case study from Bandas del Sur, Tenerife (Canary Islands). Bull. Volcanol. 75, 734. https://doi.org/10.1007/s00445-013-0734-1.

Lambeck, K., Rouby, H., Purcell, A., Sun, Y., Sambridge, M., 2014. Sea level and global ice volumes from the Last Glacial Maximum to the Holocene. Proc. Natl. Acad. Sci. U. S. A. 111, 15296. https://doi.org/10.1073/pnas.1411762111.

Lénat, J.-F., Merle, O., Lespagnol, L., 2009. La réunion: an example of channeled hot spot plume. J. Volcanol. Geotherm. Res. 184, 1–13. https://doi.org/10.1016/j.jvolgeores.2008.12.001.

Lipman, P.W., Moore, J.G., 1996. Mauna Loa lava accumulation rates at the Hilo drill site: formation of lava deltas during a period of declining overall volcanic growth. J. Geophys.Res.Solid Earth 101, 11631–11641. https://doi.org/10.1029/95JB03214.

Llanes, P., Herrera, R., Gómez, M., Muñoz, A., Acosta, J., Uchupi, E., Smith, D., 2009. Geological evolution of the volcanic island La Gomera, Canary Islands, from analysis of its geomorphology. Mar. Geol. 264, 123–139. https://doi.org/10.1016/j.margeo.2009.05.001.

Lockwood, J.P., Lipman, P.W., 1987. Holocene eruptive history of Mauna Loa Volcano. In: Volcanism in Hawaii, 1, pp. 509–535.

Longpré, M.-A., Felpeto, A., 2021. Historical volcanism in the Canary Islands; part 1: a review of precursory and eruptive activity, eruption parameter estimates, and implications for hazard assessment. J. Volcanol. Geotherm. Res. 419, 107363 https://doi.org/10.1016/j.jvolgeores.2021.107363.

Longpré, M.-A., Chadwick, J.P., Wijbrans, J., Iping, R., 2011. Age of the El Golfo debris avalanche, El Hierro (Canary Islands): new constraints from laser and furnace 40Ar/39Ar dating. J. Volcanol. Geotherm. Res. 203, 76–80. https://doi.org/10.1016/j.jvolgeores.2011.04.002.

Magnall, N., James, M.R., Tuffen, H., Vye-Brown, C., Schipper, C.I., Castro, J.M., Davies, A.G., 2018. The origin and evolution of breakouts in a cooling-limited rhyolite lava flow. GSA Bull. 131, 137–154. https://doi.org/10.1130/B31931.1.

Malin, M.C., 1980. Lengths of Hawaiian lava flows. Geology 8, 306–308. https://doi.org/10.1130/0091-7613(1980)8<306:LOHLF>2.0.CO;2.

Mangan, M.T., Cashman, K.V., 1996. The structure of basaltic scoria and reticulite and inferences for vesiculation, foam formation, and fragmentation in lava fountains. J. Volcanol. Geotherm. Res. 73, 1–18. https://doi.org/10.1016/0377-0273(96)00018-2.

Manville, V., Németh, K., Kano, K., 2009. Source to sink: a review of three decades of progress in the understanding of volcaniclastic processes, deposits, and hazards. Sediment. Geol. 220, 136–161. https://doi.org/10.1016/j.sedgeo.2009.04.022.

Maréchal, C., Boutier, A., Mélières, M.-A., Clauzel, T., Betancort, J.F., Lomoschitz, A., Meco, J., Fourel, F., Barral, A., Amiot, R., Lécuyer, C., 2020. Last Interglacial sea surface warming during the sea-level highstand in the Canary Islands: implications for the Canary Current and the upwelling off African coast. Quat. Sci. Rev. 234, 106246 https://doi.org/10.1016/j.quascirev.2020.106246.

Martin, U., Németh, K., 2006. How Strombolian is a "Strombolian" scoria cone? Some irregularities in scoria cone architecture from the Transmexican Volcanic Belt, near Volcán Ceboruco, (Mexico) and Al Haruj (Libya). J. Volcanol. Geotherm. Res. 155, 104–118. https://doi.org/10.1016/j.jvolgeores.2006.02.012.

Masson, D.G., 1996. Catastrophic collapse of the volcanic island of Hierro 15 ka ago and the history of landslides in the Canary Islands. Geology 24, 231–234. https://doi.org/10.1130/0091-7613(1996)024<0231:CCOTVI>2.3.CO;2.

Masson, D.G., Watts, A.B., Gee, M.J.R., Urgeles, R., Mitchell, N.C., Le Bas, T.P., Canals, M., 2002. Slope failures on the flanks of the western Canary Islands. Earth Sci. Rev. 57, 1–35. https://doi.org/10.1016/S0012-8252(01)00069-1.

Masson, D.G., Le Bas, T.P., Grevemeyer, I., Weinrebe, W., 2008. Flank collapse and large-scale landsliding in the Cape Verde Islands, off West Africa. Geochem. Geophys. Geosyst. 9 https://doi.org/10.1029/2008GC001983.

Mattox, T.N., Mangan, M.T., 1997. Littoral hydrovolcanic explosions: a case study of lava–seawater interaction at Kilauea Volcano. J. Volcanol. Geotherm. Res. 75, 1–17. https://doi.org/10.1016/S0377-0273(96)00048-0.

Meco, J., Lomoschitz, A., Rodríguez, Á., Ramos, A.J.G., Betancort, J.F., Coca, J., 2018. Mid and Late Holocene Sea level variations in the Canary Islands. Palaeogeogr. Palaeoclimatol. Palaeoecol. 507, 214–225. https://doi.org/10.1016/j.palaeo.2018.07.020.

Melo, C.S., Martín-González, E., da Silva, C.M., Galindo, I., González-Rodríguez, A., Baptista, L., Rebelo, A.C., Madeira, P., Voelker, A.H.L., Johnson, M.E., Arruda, S.A., Ávila, S.P., 2022. Range expansion of tropical shallow-water marine molluscs in the NE Atlantic during the last interglacial (MIS 5e): causes, consequences and utility of ecostratigraphic indicators for the Macaronesian archipelagos. Quat. Sci. Rev. 278, 107377 https://doi.org/10.1016/j.quascirev.2022.107377.

Mitchell, N.C., Dade, W.B., Masson, D.G., 2003. Erosion of the submarine flanks of the Canary Islands. J.Geophys.Res.Earth Surf. 108 https://doi.org/10.1029/2002JF000003.

Mitchell, N.C., Beier, C., Rosin, P.L., Quartau, R., Tempera, F., 2008. Lava penetrating water: submarine lava flows around the coasts of Pico Island, Azores. Geochem. Geophys. Geosyst. 9 https://doi.org/10.1029/2007GC001725.

Negredo, A.M., van Hunen, J., Rodríguez-González, J., Fullea, J., 2022. On the origin of the Canary Islands: insights from mantle convection modelling. Earth Planet. Sci. Lett. 584, 117506 https://doi.org/10.1016/j.epsl.2022.117506.

Németh, K., 2010. Monogenetic volcanic fields: origin, sedimentary record, and relationship with polygenetic volcanism. In: Special Paper of the Geological Society of America. https://doi.org/10.1130/2010.2470(04).

Newhall, C.G., Self, S., 1982. The volcanic explosivity index (VEI) an estimate of explosive magnitude for historical volcanism. J.Geophys.Res.Oceans 87, 1231–1238. https://doi.org/10.1029/JC087iC02p01231.

Noe-Nygaard, A., 1968. On extrusion forms in plateau basalts. In: Shield Volcanoes of "scutulum" Type, Vísindafélag Íslendinga Anniversary Volume, pp. 10–13.

Nunn, P., 1994. Oceanic Islands, The Natural Environment. Wiley-Blackwell, Oxford.

Osman, M.B., Tierney, J.E., Zhu, J., Tardif, R., Hakim, G.J., King, J., Poulsen, C.J., 2021. Globally resolved surface temperatures since the Last Glacial Maximum. Nature 599, 239–244. https://doi.org/10.1038/s41586-021-03984-4.

Pacheco, Hernández, 1987. El vulcanismo histórico del Archipiélago Canario: pautas temporales, espaciales, estructurales y petrológico-geoquímicas. In: Actas. Madrid, pp. 2367–2393.

Paris, R., Naylor, L.A., Stephenson, W.J., 2011. Boulders as a signature of storms on rock coasts. Mar. Geol. 283, 1–11. https://doi.org/10.1016/j.margeo.2011.03.016.

Pérez, N., Rodríguez, G., Pacheco, J.M., 2014. Atmospheric recirculation on the east coast of Gran Canaria Island. WIT Trans. Ecol. Environ. 183, 15–25. https://doi.org/10.2495/AIR140021.

Perez-Torrado, F.J., Gimeno, D., Aulinas, M., Cabrera, M.C., Guillou, H., Rodriguez-Gonzalez, A., Gisbert, G., Fernandez-Turiel, J.L., 2015. Polygonal feeder tubes filled with hydroclasts: a new volcanic lithofacies marking shoreline subaerial–submarine transition. J. Geol. Soc. 172, 29. https://doi.org/10.1144/jgs2014-040.

Pinkerton, H., Wilson, L., 1994. Factors controlling the lengths of channel-fed lava flows. Bull. Volcanol. 56, 108–120. https://doi.org/10.1007/BF00304106.

Poland, M.P., Orr, T.R., 2014. Identifying hazards associated with lava deltas. Bull. Volcanol. 76, 880. https://doi.org/10.1007/s00445-014-0880-z.

Prémaillon, M., Regard, V., Dewez, T.J.B., Auda, Y., 2018. GlobR2C2 (Global Recession Rates of Coastal Cliffs) a global relational database to investigate coastal rocky cliff erosion rate variations. Earth Surf.Dyn. 6, 651–668. https://doi.org/10.5194/esurf-6-651-2018.

Prieto-Torrell, C., Rodriguez-Gonzalez, A., Aulinas, M., Fernandez-Turiel, J.L., Cabrera, M.C., Criado, C., Perez-Torrado, F.J., 2021. In: Modelling and simulation of a lava flow affecting a shore platform: a case study of Montaña de Aguarijo eruption, El Hierro (Canary Islands, Spain), 17, pp. 502–511. https://doi.org/10.1080/17445647.2021.1972853 null.

Pugh, D., Woodworth, P., 2014. Sea-level Science: Understanding Tides, Surges, Tsunamis And Mean Sea-level Changes. Cambridge University Press.

Quartau, R., Trenhaile, A.S., Mitchell, N.C., Tempera, F., 2010. Development of volcanic insular shelves: Insights from observations and modelling of Faial Island in the Azores Archipelago. Mar. Geol. 275, 66–83. https://doi.org/10.1016/j.margeo.2010.04.008.

Quartau, R., Hipólito, A., Romagnoli, C., Casalbore, D., Madeira, J., Tempera, F., Roque, C., Chiocci, F., 2014. The morphology of insular shelves as a key for understanding the geological evolution of volcanic islands: insights from Terceira Island (Azores). Geochem. Geophys. Geosyst. 15, 1801–1826. https://doi.org/10.1002/2014GC005248.

Quartau, R., Madeira, J., Mitchell, N.C., Tempera, F., Silva, P.F., Brandão, F., 2015. The insular shelves of the Faial-Pico Ridge (Azores archipelago): a morphological record of its evolution. Geochem. Geophys. Geosyst. 16, 1401–1420. https://doi.org/10.1002/2015GC005733.

Ramalho, R., Helffrich, G., Cosca, M., Vance, D., Hoffmann, D., Schmidt, D.N., 2010. Episodic swell growth inferred from variable uplift of the Cape Verde hotspot islands. Nat. Geosci. 3, 774–777. https://doi.org/10.1038/ngeo982.

Ramalho, R.S., Quartau, R., Trenhaile, A.S., Mitchell, N.C., Woodroffe, C.D., Ávila, S.P., 2013. Coastal evolution on volcanic oceanic islands: a complex interplay between volcanism, erosion, sedimentation, sea-level change and biogenic production. Earth Sci. Rev. 127, 140–170. https://doi.org/10.1016/j.earscirev.2013.10.007.

Rijsdijk, K.F., Hengl, T., Norder, S.J., Ávila, S.P., Fernández-Palacios, J.M., 2013. Modelling sea level driven change of Macaronesian archipelago configurations since 120 kyr BP.

Risica, G., Di Roberto, A., Speranza, F., Carlo, P.D., Pompilio, M., Meletlidis, S., Todrani, A., 2022. Reconstruction of the subaerial Holocene volcanic activity through paleomagnetic and 14C dating methods: El Hierro (Canary Islands). J. Volcanol. Geotherm. Res. 425, 107526 https://doi.org/10.1016/j.jvolgeores.2022.107526.

Rodríguez, G., Nistal, A., Pérez, B., 1999. Joint occurrence of high tide, surge and storm-waves on the northwest Spanish coast. Bol. Inst. Esp. Oceanogr. 15, 21–29.

Rodriguez-Gonzalez, A., Fernandez-Turiel, J.L., Perez-Torrado, F.J., Gimeno, D., Aulinas, M., 2010. Geomorphological reconstruction and morphometric modelling applied to past volcanism. Int. J. Earth Sci. 99, 645–660. https://doi.org/10.1007/s00531-008-0413-1.

Rodriguez-Gonzalez, A., Fernandez-Turiel, J.L., Perez-Torrado, F.J., Aulinas, M., Carracedo, J.C., Gimeno, D., Guillou, H., Paris, R., 2011. GIS methods applied to the degradation of monogenetic volcanic fields: a case study of the Holocene volcanism of Gran Canaria (Canary Islands, Spain). Geomorphology 134, 249–259. https://doi.org/10.1016/j.geomorph.2011.06.033.

Rodriguez-Gonzalez, A., Fernandez-Turiel, J.L., Perez-Torrado, F.J., Paris, R., Gimeno, D., Carracedo, J.C., Aulinas, M., 2012a. Factors controlling the morphology of monogenetic basaltic volcanoes: the Holocene volcanism of Gran Canaria (Canary Islands, Spain). Geomorphology 136, 31–44. https://doi.org/10.1016/j.geomorph.2011.08.023.

Rodriguez-Gonzalez, A., Perez-Torrado, F.J., Fernandez-Turiel, J.L., Carracedo, J.C., Guillou, H., 2012. Modelado geomorfológico con técnicas SIG de erupciones volcánicas generadoras de plataformas costeras: el volcán de Montaña del Tesoro(El Hierro, Islas Canarias). In: Geotemas.

Rodriguez-Gonzalez, A., Perez-Torrado, F.J., Fernandez-Turiel, J.L., Aulinas, M., Paris, R., Moreno-Medina, C., 2018. The Holocene volcanism of Gran Canaria (Canary Islands, Spain). J.Maps 14, 620–629. https://doi.org/10.1080/17445647.2018.1526717.

Roeser, H.A., 1982. Magnetic anomalies in the magnetic quiet zone off Morocco. In: von Rad, U., Hinz, K., Sarnthein, M., Seibold, E. (Eds.), Geology of the Northwest African Continental Margin. SpringerBerlin Heidelberg, Berlin, Heidelberg, pp. 61–68.

Roest, W.R., Dañobeitia, J.J., Verhoef, J., Collette, B.J., 1992. Magnetic anomalies in the canary basin and the Mesozoic evolution of the central North Atlantic. Mar. Geophys. Res. 14, 1–24. https://doi.org/10.1007/BF01674063.

Romero Ruiz, M.del C., 1990. Las manifestaciones volcánicas históricas del Archipiélago Canario. Universidad de La Laguna, La Laguna (PhD Thesis).

Ryan, W.B.F., Carbotte, S.M., Coplan, J.O., O'Hara, S., Melkonian, A., Arko, R., Weissel, R.A., Ferrini, V., Goodwillie, A., Nitsche, F., Bonczkowski, J., Zemsky, R., 2009. Global Multi-Resolution Topography synthesis. Geochem. Geophys. Geosyst. 10 https://doi.org/10.1029/2008GC002332.

Schmincke, H.-U., Sumita, M., 2010. Geological Evolution of the Canary Islands: A Young Volcanic Archipelago Adjacent to the Old African Continent. Görres-Verlag, Koblenz.

Semedo, A., Sušelj, K., Rutgersson, A., Sterl, A., 2011. A global view on the wind sea and swell climate and variability from ERA-40. J. Clim. 24, 1461–1479. https://doi.org/10.1175/2010JCLI3718.1.

Silver, P.G., Raymond, M.Russo, Carolina, Lithgow-Bertelloni, 1998. Coupling of South American and African Plate motion and Plate deformation. Science 279, 60–63. https://doi.org/10.1126/science.279.5347.60.

Smellie, J.L., Wilch, T.I., Rocchi, S., 2013. 'A'ā lava-fed deltas: a new reference tool in paleoenvironmental studies. Geology 41, 403–406. https://doi.org/10.1130/G33631.1.

Soule, S.A., Zoeller, M., Parcheta, C., 2021. Submarine lava deltas of the 2018 eruption of Kīlauea volcano. Bull. Volcanol. 83, 23. https://doi.org/10.1007/s00445-020-01424-1.

Stephenson, W.J., Dickson, M.E., Trenhaile, A.S., 2013. 10.11 rock coasts. In: Shroder, J. F. (Ed.), Treatise on Geomorphology. Academic Press, San Diego, pp. 289–307. https://doi.org/10.1016/B978-0-12-374739-6.00284-0.

Sun, W., Langmuir, C.H., Ribe, N.M., Zhang, L., Sun, S., Li, H., Li, C., Fan, W., Tackley, P. J., Sanan, P., 2021. Plume-ridge interaction induced migration of the Hawaiian-Emperor seamounts. Sci.Bull. 66, 1691–1697. https://doi.org/10.1016/j.scib.2021.04.028.

Sunamura, T., 1992. Geomorphology of rocky coasts. In: Coastal Morphology And Research. Wiley, New York.

Sunamura, T., 2015. Rocky coast processes: with special reference to the recession of soft rock cliffs. Proc.Jpn. Acad.Ser.B 91, 481–500. https://doi.org/10.2183/pjab.91.481.

Thouret, J.-C., 1999. Volcanic geomorphology—an overview. Earth Sci. Rev. 47, 95–131. https://doi.org/10.1016/S0012-8252(99)00014-8.

Tibaldi, A., 1995. Morphology of pyroclastic cones and tectonics. J.Geophys.Res.Solid Earth 100, 24521–24535. https://doi.org/10.1029/95JB02250.

Trenhaile, A.S., 2010. The effect of Holocene changes in relative sea level on the morphology of rocky coasts. Geomorphology 114, 30–41. https://doi.org/10.1016/j.geomorph.2009.02.003.

Trenhaile, A.S., 2016. Cliffs and rock coasts☆. In: Reference Module in Earth Systems And Environmental Sciences. Elsevier. https://doi.org/10.1016/B978-0-12-409548-9.09737-2.

Trenhaile, A.S., Kanyaya, J.I., 2007. The role of wave erosion on sloping and horizontal shore platforms in macro- and mesotidal environments. J. Coast. Res. 2007, 298–309. https://doi.org/10.2112/04-0282.1.

Urgeles, R., Canals, M., Baraza, J., Alonso, B., Masson, D., 1997. The most recent megalandslides of the Canary Islands: El Golfo debris avalanche and Canary debris flow, west El Hierro Island. J.Geophys.Res.Solid Earth 102, 20305–20323. https://doi.org/10.1029/97JB00649.

Vega, G., Salas, J., Dominguez, N., 2021. Lava from the volcanic eruption on La Palma reaches the sea. In: El País.

Walker, G.P.L., 1972. Compound and simple lava flows and flood basalts. Bull. Volcan. Ser. Ill 35, 579–590.

Walker, G.P.L., 2000. Basaltic volcanoes and volcanic systems. In: Encyclopedia of Volcanoes. Academic Press, pp. 283–289.

Warren, S.D., Hohmann, M.G., Auerswald, K., Mitasova, H., 2004. An evaluation of methods to determine slope using digital elevation data. Catena 58, 215–233. https://doi.org/10.1016/j.catena.2004.05.001.

Watts, A.B., Masson, D.G., 1995. A giant landslide on the north flank of Tenerife, Canary Islands. J.Geophys.Res.Solid Earth 100, 24487–24498. https://doi.org/10.1029/95JB02630.

The Puu Oo eruption of Kilauea Volcano, Hawaii; episodes 1 through 20, January 3, 1983, through June 8, 1984. In: Wolfe, E.W. (Ed.), 1988. U. S. Geol. Surv. Prof. Pap, 1463, pp. 1–251. https://doi.org/10.3133/pp1463.

Woodroffe, C.D., 2014. Chapter 15 the rock coasts of oceanic islands. In: Geological Society, London, Memoirs, 40, p. 247. https://doi.org/10.1144/M40.15.

Young, A.P., Carilli, J.E., 2019. Global distribution of coastal cliffs. Earth Surf. Process. Landf. 44, 1309–1316. https://doi.org/10.1002/esp.4574.

Zaczek, K., Troll, V.R., Cachao, M., Ferreira, J., Deegan, F.M., Carracedo, J.C., Soler, V., Meade, F.C., Burchardt, S., 2015. Nannofossils in 2011 El Hierro eruptive products reinstate plume model for Canary Islands. Sci. Rep. 5, 7945. https://doi.org/10.1038/srep07945.

Zhao, Z., Mitchell, N.C., Quartau, R., Tempera, F., Bricheno, L., 2019. Submarine platform development by erosion of a Surtseyan cone at Capelinhos, Faial Island, Azores. Earth Surf. Process. Landf. 44, 2982–3006. https://doi.org/10.1002/esp.4724.

Zhao, Z., Mitchell, N.C., Quartau, R., Ramalho, R.S., Rusu, L., 2020. Coastal erosion rates of lava deltas around oceanic islands. Geomorphology 370, 107410. https://doi.org/10.1016/j.geomorph.2020.107410.